Interfacial Thermal Fluid Phenomena in Thin Liquid Films

Oleg A. Kabov
Institute of Thermophysics SB RAS, Novosibirsk, Russia, Email: kabov@itp.nsc.ru
Universite Libre de Bruxelles, Microgravity Research Center, Bruxelles, Belgium
Heat Transfer International Research Institute of Universite Libre de Bruxelles and Institute of Thermophysics of Russian Academy of Sciences, Brussels, Belgium, okabov@ulb.ac.be
Center of Smart Interfaces, Technische Universität Darmstadt, Darmstadt, Germany

ABSTRACT
Films are ubiquitous in nature and play an important role in our daily life. The paper focuses on the recent progress that has been achieved in the interfacial thermal fluid phenomena in thin liquid films and rivulets through conducting experiments and theory. Phase shift schlieren technique, fluorescence method and infrared thermography have been used. A spanwise regular structures formation was discovered for films falling down an inclined plate with a built-in local rectangular heater. If the heating is low enough, a stable 2D flow with a bump at the front edge of the heater is observed. For lager heat flux this primary flow becomes unstable, and the instability leads to another steady 3D flow, which looks like a regular structure with a periodically bent leading bump and an array of longitudinal rolls or rivulets descending from it downstream. The heat flux needed for the onset of instability grows almost linearly with the increase of Re number. Strong surface temperature gradients up to 10–15 K/mm, both in the streamwise and spanwise directions have been measured. For a wavy film it was found that heating may increase the wave amplitude because thermocapillary forces are directed from the valley to the crest of the wave. Thin and very thin (less than 10 μm) liquid films driven by a forced gas/vapor flow (stratified or annular flows), i.e. shear-driven liquid films in a narrow channel are a promising candidate for the thermal management of advanced semiconductor devices in earth and space applications. Development of such technology requires significant advances in fundamental research, since the stability of joint flow of locally heated liquid film and gas is a rather complex problem. Experiments with water and FC-72 in flat channels (height 0.2–2 mm) have been conducted. Maps of flow regimes were plotted. It was found that stratified flow exists and stable in the channels with 0.2 mm height and 40 mm width. The critical heat flux for a shear driven film may be up to 10 times higher than that for a falling liquid film, and reaches 400 W/cm^2 in experiments with water at atmospheric pressure. Some experiments have been done during parabolic flight campaigns of the European Space Agency under microgravity conditions. It was found that decreasing of gravity leads to a flow destabilization.

Keywords: liquid films, thermocapillary effects, critical heat flux.

Nomenclature

A	dimensionless criterion, No Unit
B_h	width of the heating element, m
Bi_i	biot numbers, No Unit
b_i	heat transfer coefficients, W/(m^2 K)
C	dimensionless criterion; concentration of aqueous solution of ethanol No Unit, %
CHF	critical heat flux, W/cm^2
c_p	specific heat capacity of the liquid, J/(kg K)
$\mathbf{D}$	velocity deformation tensort, No Unit
D	dimensionless criterion, No Unit

D_h	channel equivalent diameter, m
d, H	channel height, mm
Fr	Froude number, No Unit
g	gravitational acceleration, m/s^2
G	specific mass flow rate, kg/m^{2}s
h	local dimensionless film thickness or heat transfer coefficient, No Unit; W/m^{2}K
H	local dimensional film thickness, m
K	double mean curvature of the interface, m^{-1}
Kp	dimensionless criterion $= -q_{idp}\,(d\sigma/dT)/(\lambda\,\rho\,(g\sin\Theta\,\nu)^{2/3})$, No Unit
l	scale of streamwise length, m
L	heater length, m
l_ν	viscosity-gravitational interaction scale $= (\nu^2/g\sin\Theta)^{1/3}$, m
l_σ	capillary-gravitational interaction scale $= (\sigma/(\rho g\sin\Theta))^{1/2}$, m
l_δ	critical film thickness scale $= (l_\sigma^2 l_\nu^3)^{1/5}$, m
Ma	Marangoni number, No Unit
$\vec{n}$	unit vector of the outward normal to the free surface
p	Pressure, N/m^2
q	heat flux released on the heater, W/cm^2
q_{idp}	threshold heat flux at which an initial stable dry patch forms, W/m^2
q_{rol}	density of heat flux for structures formation, W/cm^2
Q	characteristic scales for temperature; Volumetric flow rate, K/m; m^3/s
Re	Reynolds number, $= \Gamma\rho/\mu$, No Unit
t	Time, s
T	Temperature, °C
U	scale of the liquid velocity, m/s
U_S	superficial velocity $= \Gamma/H$, m/s
u, v, w	velocity components, m/s
ν	velocity vector, m/s
W_f	film flow width, m
x, y, z	Cartesian coordinates, m
X_n	distance from the nozzle to the heater, m
X_t	distance from the upper edge of the heater, m

Greek symbols

Γ	specific volumetric flow rate, m^2/s
α, Θ	plate inclination angle, degree
ε	small parameter, No Unit
θ	dimensionless temperature, No Unit
κ	thermal conductivity, W/(m K)
λ	pressure drop, N/m^2
$\mu = \mu(T)$	liquid dynamic viscosity, kg/(m s)
ξ	dimensionless variable, No Unit
ρ	Density, kg/m^3
σ	surface tension, N/m
$\vec{\tau} = (\tau,0,0)$	tangential stress, N/m^2

Subscripts

g, l	gas and liquid
0	initial parameters of the flow, (at $T = T_0$)
1, 2	in the substrate and gas, respectively
x, y, z, t, ξ, T	derivations on x, y, z, t, ξ and T
W	wall (heater)

Superscripts

1	new variable

1. INTRODUCTION

The heat transfer, dynamics, stability and rupture of thin liquid films and rivulets with and without phase-change have fascinated scientists over many decades. Films are ubiquitous in nature and play an important role in our daily life (meandering rivulets [1], fingering instability of a moving contact line [2], regular wave patterns [3]). Film flows occur over a wide range of flow rates (Re = $10^{-2} - 10^{6}$) and length scales ($10^{-6} - 10^{3}$ m) and are central to several areas of engineering, geophysics, and biophysics; these include cooling technologies, nanofluidics, microfluidics, and coating, waterfalls, and lava flows, corneal tear-film, and thin liquid film of lung.

In case of a thin liquid film non-uniformly heated the action of Marangoni effect resulting from the large temperature gradients at the liquid-gas interface induces structural changes in the pattern of the flow that may lead to increasing or decreasing of the heat transfer coefficient and film rupture. The thermocapillary effects on gravitationally driven falling liquid film on a solid plate have been studied theoretically by Joo et al. [4], Kalliadasis et al. [5] and by Miladinova et al. [6] for uniformly and non-uniformly heated plate. For a current review of the field see also paper by Oron et al. [7], as well as books by Alekseenko et al. [8] and Demekhin and Chang [9].

Some experimental studies executed in [10–15] have focused their efforts on thin films falling down along locally heated plates and have revealed the occurrence of novel effects: the phenomenon of "rivulet structures", the phenomenon of "horizontal bump" and the phenomenon of "lateral waves". In order to explain the horizontal bump and other phenomena in locally heated liquid films, two-dimensional and three-dimensional models are proposed in the papers [16–25] taking into account variations of surface tension with temperature. In some papers variation of liquid viscosity with temperature also has been taken into account [12, 14, 23, 24, 25].

Film flows also present in space applications: energy production, electronic cooling devices, life support systems and waste water treatment for long duration space exploration missions [26]. Some experimental studies executed in [27] have focused their efforts on thin films dynamics under microgravity conditions and have found that decreasing of gravity leads to a flow destabilization.

In recent years, increasing performance demands in semiconductor technology, including shrinking feature size, increasing transistor density, and faster circuit speeds, have resulted in very high chip power dissipation and heat fluxes. It is also leading to greater non-uniformity of on-chip power dissipation, creating localized, sub-millimeter hot spots, often exceeding 1kW/cm^2 in heat flux, which can degrade the processor performance and reliability [28, 29]. Similar developments are underway in microwave integrated circuits and Power Amplifier chips, with even higher localized heat fluxes and heat densities.

The forced flow of dielectric liquids, undergoing phase change while flowing in a narrow channel, is a promising candidate for the thermal management of advanced semiconductor devices in terrestrial and space applications [30]. Such channels may be created by the spacing between silicon ribs in a microchannel cooler, between stacked silicon chips in a three-dimensional logic, or heterogeneous microsystem, narrowly-spaced organic or ceramic substrates, and between a chip and a non-silicon polymer cover in a microgap cooler [31]. These microgap configurations provide direct contact and hence cooling between a chemically-inert, dielectric liquid and the back surface of an active electronic component, thus eliminating the significant thermal resistance associated with a Thermal Interface Material or the solid-solid contact resulting from the attachment of a microchannel cold-plate to the chip. While direct contact cooling is thermally very efficient, in such configurations, it is the poorly understood two-phase flow phenomena that establish the upper bound on the heat removal capability.

Two-phase flow in miniature channels is dominated by annular flow, with thin liquid films flowing along the walls and a vapor core in the center [30]. The behavior of such thin and very thin (less than 10 μm) liquid film, whether driven by a forced gas/vapor flow as in annular flows [30, 31, 32] or pseudo-stratified flows [33, 34, 35, 36, 37]), i.e. shear-driven liquid film in a narrow channel (100–300 μm [38]) is at the heart of the thermal performance of such microgap coolers.

It is quite evident that the combined effects of evaporation, thermocapillarity, gas dynamics, and gravity as well as the formation of microscopic adsorbed film on the wall, are somewhat complicated issues and have not yet been studied systematically. The present work will provide an overview of the recent progress that has been achieved in the experimental and theoretical aspects of such flows. By performing experiments in space without the interference of gravity, it is possible to provide the basics required to formulate precise models and support the optimisation of system designs. Part of the present work is devoted to the recent experiments in microgravity conditions.

2. FALLING LIQUID FILMS AT LOCAL HEATING

2.1. Flow Regimes in Falling Locally Heated Liquid Film

Experimental studies executed by Kabov and his colleagues [10–15] have focused their efforts on thin films falling down along locally heated plates and have revealed the occurrence of novel effects: the phenomenon of "rivulet structures" [10, 11, 13], the phenomenon of "horizontal bump" [12, 15] and the phenomenon of "lateral waves" [11, 14], Fig. 2.1.

Local heaters with different sizes are used. The temperature conditions of the liquids vary from highly subcooled to up to close to saturation. Low Reynolds number flows corresponding to film thickness of about 50–100 μm and high temperature gradients on the liquid-gas interface have been studied. As the temperature of the fluid surface increases, the surface tension decreases, the resulting surface tension gradient produces a Marangoni flow opposed to the gravitationally driven flow, Fig. 2.2.

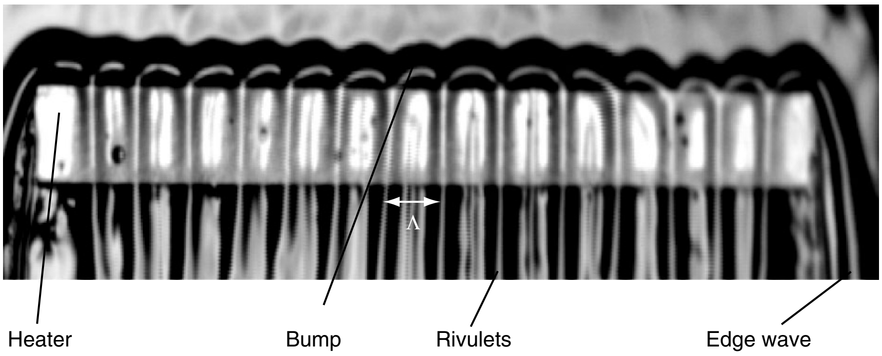

Figure 2.1. Structure of falling liquid film at local heating, 10% ethyl-alcohol in water, heater 6.75×109 mm^2, Re = 1, $q_{rol} = 1.73$ W/cm^2.

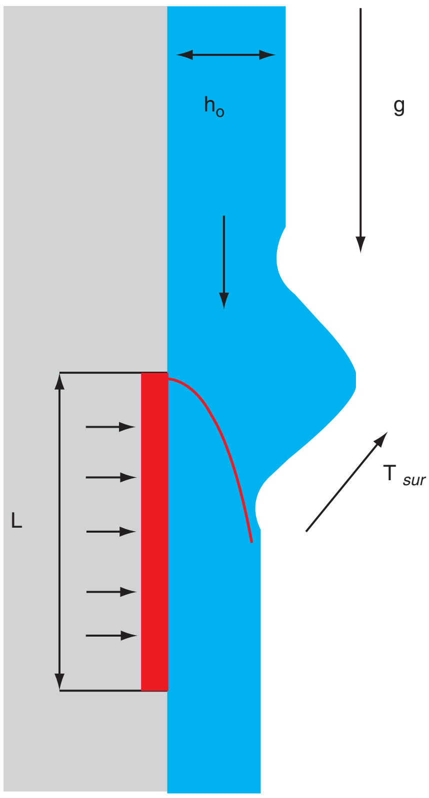

Figure 2.2. Schematic of liquid film flow at local heating.

2.1.1. Experimental Setup

A photograph and a schematic of one of experimental test section are shown in Figs. 2.3, 2.4, respectively. The main plate is made of the $46 \times 214 \times 250$ mm^3 textolite block. Inside the main plate there is a temperature stabilizer as the system of channels with the diameter of 8 mm, through which the working

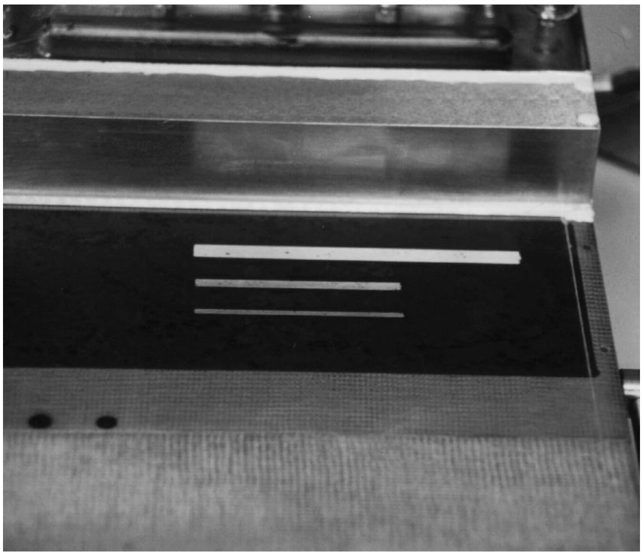

Figure 2.3. A photograph of experimental test section.

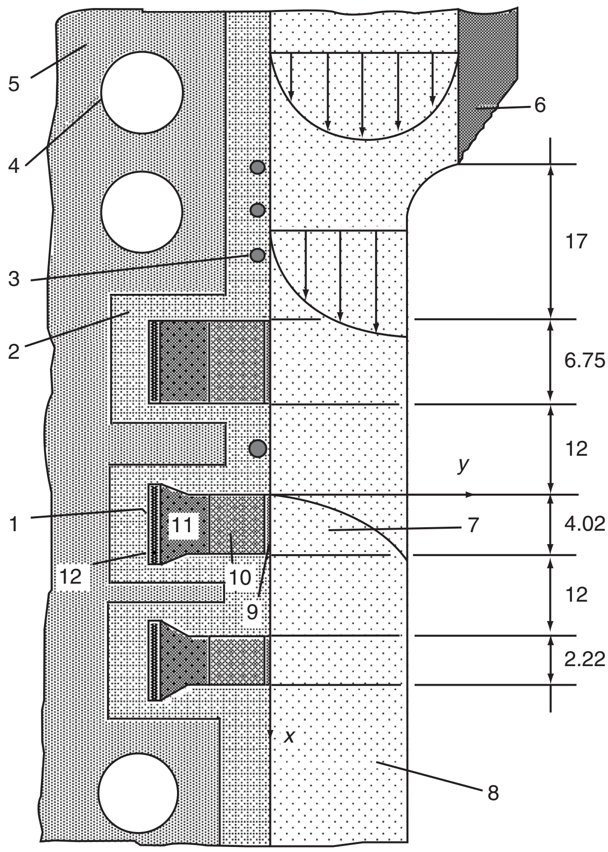

Figure 2.4. The schematic of experimental test section. 1- heater, 2- heat-insulating mixture, 3-thermocouple, 4- temperature stabilizer, 5- textolite plate, 6- nozzle, 7- heat boundary layer, 8- liquid film, 9- tin layer, 10- stainless steel plate, 11- copper block, 12- electrical heat source.

liquid is pumped. The liquid flow width is 200 mm. The nozzle gap height is equal to 270 μm. The test section includes three heaters with different size (6.75 × 109 mm, 4.02 × 68 mm and 2.22 × 68 mm).

The heat source consists of electric heater, copper block and stainless steel plate covered with a layer of tin 100–150 μm thick. The 2-mm wide cavity around the heater is filled with the mixture of epoxy resin and charcoal powder with thermal conductivity around 100 times less than that of stainless steel. The 2.5-mm layer of the same mixture is also covered the surface around the heater with the size of 85 × 200 mm^2 (black area in Fig. 2.3). The surface of the plate as well as the heaters is finely polished. The distance from the nozzle to the heat source is chosen such that on the one hand, the film reaches the heater with the stabilized velocity profile and thickness, and on the other hand, the heating units are located in the region of smooth waveless film flow [8].

The experiments are carried out under the atmospheric pressure in stationary conditions. The liquid is highly subcooled up to the saturation temperature. The initial temperature of the film is ranged from 4° to 20°C. The inclination angle is set with the help of goniometer with accuracy of 0.1 degree. For the flow visualization a reflection Schliren and IR techniques are used. The more detailed description of the equipment, test sections and investigation methods are available in [10, 12, 13, 15, 39, 40, 41, 42].

2.1.2. 2D Flow in a Bump at the Front Edge of the Heater

A liquid bump is formed in the region of the upper edge of the heating element, Fig. 2.5a. Beyond a critical heat flux, rivulets aligned with the flow start from this bump and distribute spanwise with a fixed wavelength, Fig. 2.5b and Fig. 2.5c. Two lateral (edge) waves are also formed at the lateral edges of the heating element by the spanwise Marangoni forces.

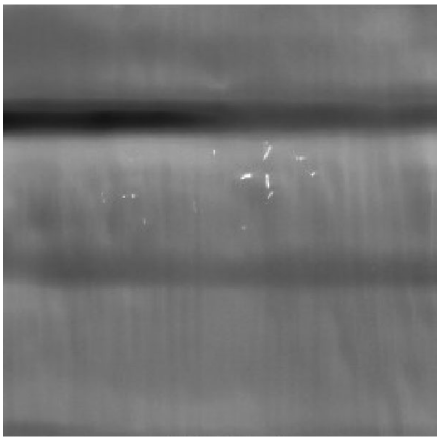

(a) $q = 0.63$ W/cm^2

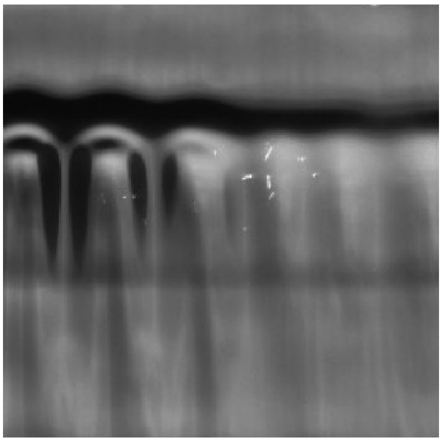

(b) $q = 1.21$ W/cm^2

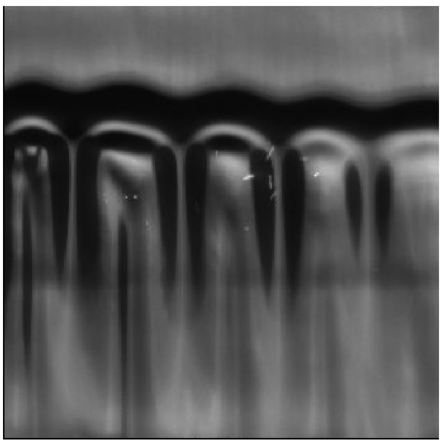

(c) $q = q_{rol} = 1.5$ W/cm^2

Figure 2.5. The liquid film deformation on the substrate with the local heater 6.7 × 68 mm^2 [12], solution of 25% ethyl alcohol in water, $T_0 = 20°\ C$, Re = 0.5, $H_0 = 0.1$ mm, inclination angle = 90°. a) horizontal bump, b)-c) rivulet structures.

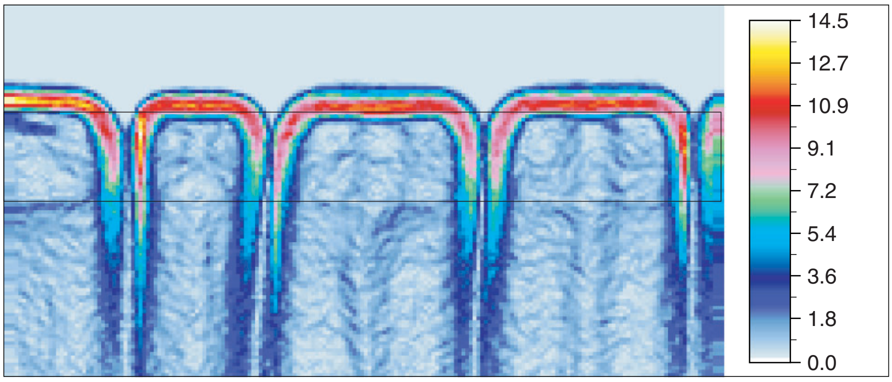

Figure 2.6. Temperature gradient on the film surface.

The onset of a horizontal liquid bump in the upper heater edge zone is common to all the experiments on thin films falling down non-uniformly heated plates [10–15]. Using the infrared thermography it is established in [10] that the formation of the bump has a thermocapillary nature. A region with maximum surface temperature gradients up to 15 K/mm appears in the bump zone, Fig. 2.6.

In [12] and [15] with the help of the Schlieren method and a double-fiber optical probe film thickness profiles have been obtained for Re number ranging from 0.09 to 3.6 and for a 6.7×68 mm^2 heater. The experiments are performed on vertical and inclined plates with aqueous solution of ethyl alcohol (mass concentration 10% and 25%). The plate inclination angle varies from 4° to 90°. Deformation of the film as a bump at the top edge of the heater has been proved to exist since the smallest heat fluxes. With increasing the heat flux the height of the bump grows.

2.1.3. Spanwise Regular Structures Formation

The critical heat flux for spanwise regular structures formation have been studied in [11, 39]. Using a hypothesis of local motionless of the film surface at the moment of structures formation due to gravitational and surface tension forces balance an equation for condition of structures formation have been written in the form:

$$Km = C_h \,\mathrm{Re}^{\mathrm{m}} (\sin\alpha)^{\mathrm{P}},$$

$$K_m = \frac{\tau_T}{\tau_w} = -\frac{d\sigma}{dT}\frac{q_{rol}}{c_p \mu}\frac{1}{\rho (g\nu)^{2/3}}$$

where q_{rol} - density of heat flux for structures formation, W/cm^2; $C_h = 2\sqrt[3]{3} = 2.88$; $m = 4/3$; $p = 2/3$. Value τ_T is the scale of thermocapillary tangential stress on the liquid interface. Value τ_g is the scale of tangential force on a wall at the purely gravity driven flow (force on the wall for a not heated film is defined by relation $\tau_W = \rho(g\nu)^{2/3}(3\mathrm{Re})^{1/3}(\sin\Theta)^{2/3}$ [43]). In Fig. 2.7 the non-dimensional critical heat flux for spanwise regular structures formation is shown versus Reynolds number for different liquids, temperatures and plate inclination angles. Known experimental data are generalized by relation:

$$Km_{rol} = 0.53\,\mathrm{Re}^{1.1}(\sin\alpha)^{0.54}$$

The critical Marangoni number, $\mathrm{Ma}_{\mathrm{cr}}$, for spanwise regular structures formation also have been studied theoretically and experimentally in [24]. Qualitatively the same tendency was observed for the smaller heating element (2.22×68.05 mm^2). It was found that the growth rate of $\mathrm{Ma}_{\mathrm{cr}}$ is lower for the small Re values (less than 0.5).

Study using the infrared thermography has been done in [10, 40, 41]. Temperature distribution on the gas-liquid interface give a possibility to culculate a field of surface temperature gradients and then a field of thermocapillary forses. Temperature and tangential stress fields on the surface of the film are shown in Fig. 2.8. The maximum temperature gradient is equal to 14.5 K/mm that is corresponds to the maximum tangential stress on the gas-liquid interface equal to 1.6 N/m^2. This value exceeds the tangential stress on the substrate for isothermal liquid film on 61%. Tangential stress before the

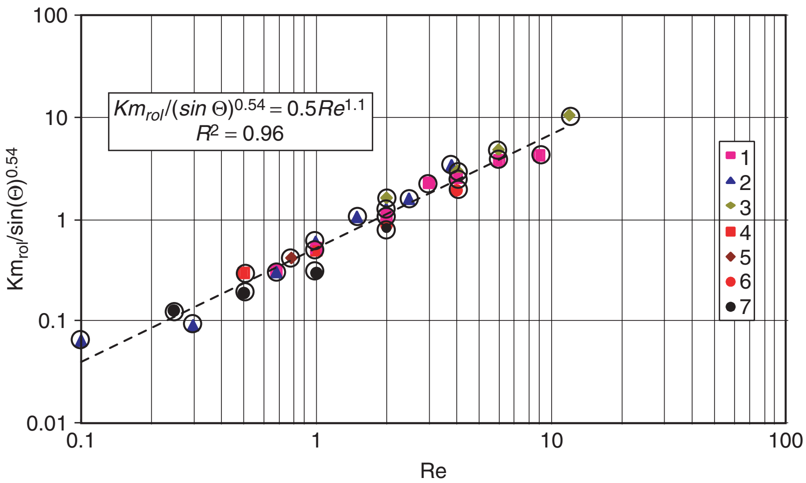

Figure 2.7. The non-dimensional critical heat flux for spanwise regular structures formation versus Reynolds number, 1- 25% ethyl alcohol solution in water, $T_0 = 30°C$, $\Theta = 90°$, heater 6.5 × 13 mm, 2- 25% ethyl alcohol solution in water, $T_0 = 17°C$, $\Theta = 4°$, heater 6.5 × 13 mm, 3- perfluorine-triethyl-amine, $T_0 = 30°C$, $\Theta = 90°$, heater 6.5 × 13 mm, 4- 10% aqueous solution of ethanol, $T_0 = 17°C$, $\Theta = 90°$, 6.75 × 109 mm, 5- 10% aqueous solution of ethanol, $T_0 = 8°C$, $\Theta = 90°$, 6.75 × 109 mm, 6- 10% aqueous solution of ethanol, $T_0 = 20°C$, $\Theta = 90°$, 6.75 × 109 mm, 7- 25% aqueous solution of ethanol, $T_0 = 20°C$, $\Theta = 90°$, 6.7 × 68 mm.

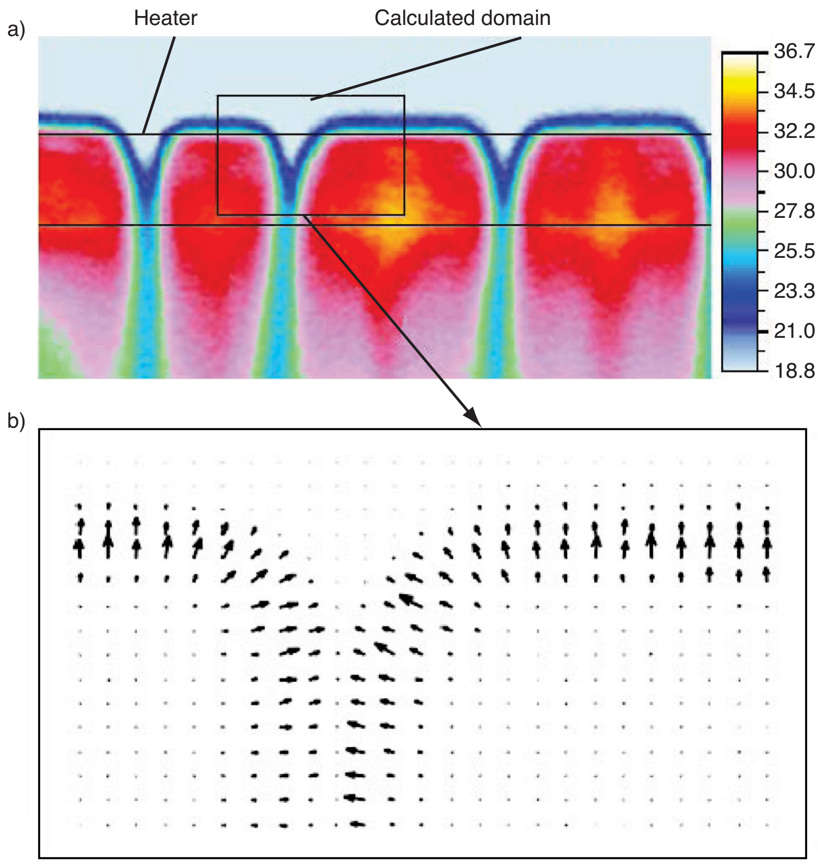

a) Temperature, b) Field of tangential stresses, Re = 1, C = 10%, $T_0 = 17°C$ °C.

Figure 2.8. Temperature and tangential stress fields on the surface of the film.

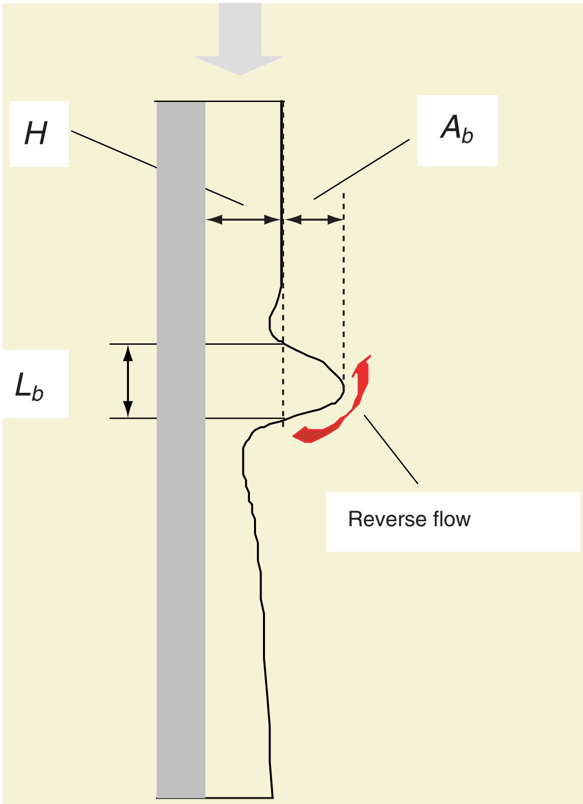

Figure 2.9. Schematic of the liquid bump formation in the falling liquid film at local heating.

instability onset is directed oposit to the main flow (Fig. 2.2) that couse a stagnation line with zero velocity on the gas-liquid interface in the bump zone, Fig. 2.9.

2.1.4. Reverse Flow in the Liquid Bump

The surface flow is made visible by aluminium tracers blown on the interface in [13]. Beyond a critical heat flux the two-dimensional flow is broken in the vicinity of the heating element leading to a strongly non-linear three-dimensional flow. A stagnation line in the bump zone has been observed.

Schematic of the liquid bump formation in the falling liquid film at local heating is shown in Fig. 2.9. Theoretical study in [24] for the heating element with the size 2.22×68.05 mm^2 shows that the 2D bump width, L_b, at the critical Marangoni number (different for each Re) is almost invariant and weakly decreasing with Re.

It was found in [12] experimentally and theoretically using a 2D model that the instability of the bump occurs when its dimensionless height, A_b, is about 0.3, and this is always accompanied by onset of the reverse flow. The dimensionless critical height of 2D bump at the onset of instability versus Reynolds number according to [24] is plotted in Fig. 2.10.

The bump height decreases almost inversely with Re. The 3D calculations confirm that the reverse flow arises when the bump height is around 0.3 and higher. Nevertheless, as for the dimensionless critical height of the bump, it strongly depend on Re and the reverse flow appearance is not a criterion of the instability onset. It was found also that an increase of surface tension leads to an increase of the bump width, L_b, and the critical Marangoni number, Ma_{cr}. The aspect ratio L_b/A_b for a critical bump varies from 62 at Re = 0.1 to 202 at Re = 1 and practically not depend on surface tension.

2.1.5. Critical Structure Width

The influence of Reynolds number on the critical structure width, Λ, has been performed in [10, 24, 44, 45]. The experiments were carried out on the vertical surface with the 6.5×13 mm^2 local heater. The law $\Lambda \sim Re^{0.06}$ was measured for the 25 % alcohol water solution and Re number variation from

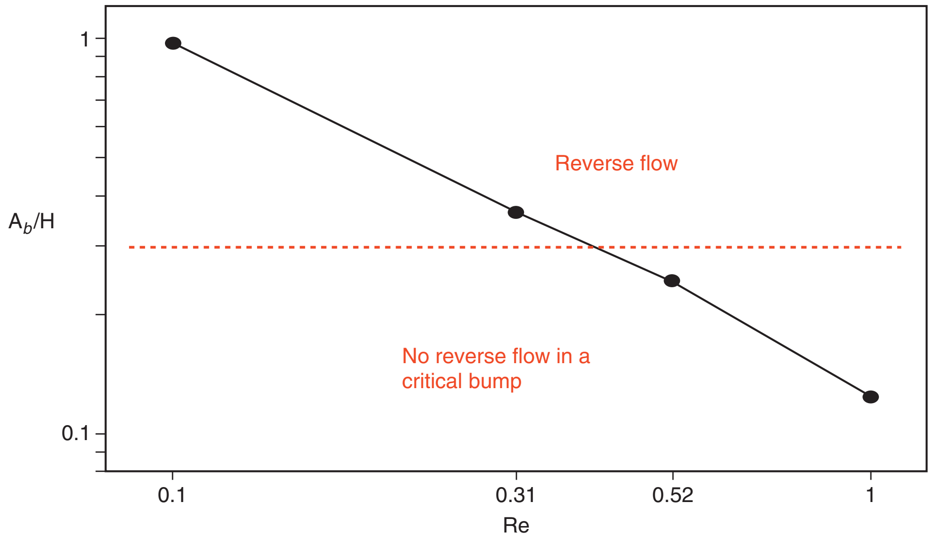

Figure 2.10. The dimensionless heights of 2D bump at the onset of instability vs Reynolds number, [24].

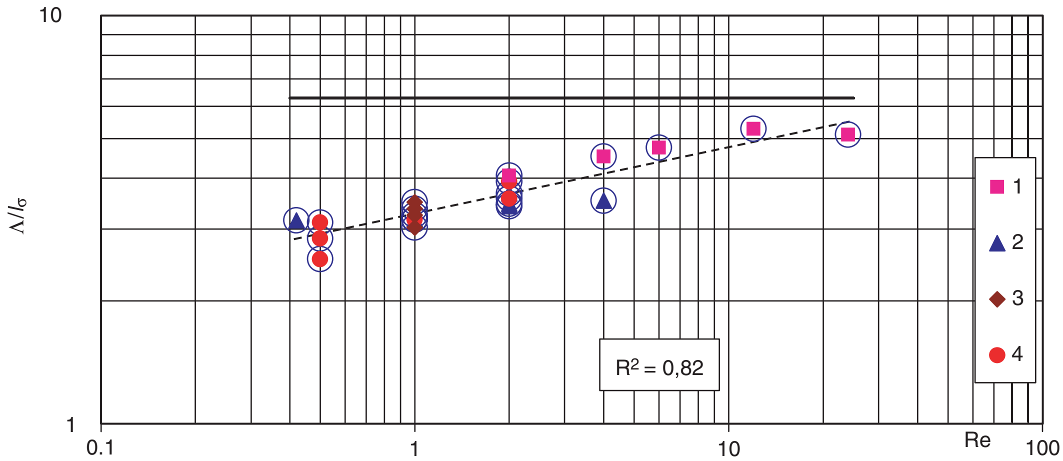

Figure 2.11. Dimensionless critical structure width versus Re number. 1- perfluorine-triethyl-amine, 6.5 × 13 mm, T_0 = 30°C [44]; 2- 25% ethyl alcohol solution, 6.5 × 13 mm, T_0 = 30°C[10]; 3- 10% ethyl alcohol solution, L = 2.22-6.75, B = 68-109 mm, T_0 = 17°C; 4- 10% ethyl alcohol solution, 6.7 × 68 mm, T_0 = 17°C; dashed line – dependence $\Lambda/l_\sigma = 3.26\mathrm{Re}^{1/6}$; horizontal line – $\Lambda/l_\sigma = 2\pi$ (critical wavelength for Rayleigh-Taylor instability [46,47]).

0.42 to 4, [10]. For the low-boiling fluid perfluortriethylamine and Re number within the range of 2-24 the dependence $\Lambda \sim \mathrm{Re}^{0.1}$ was observed, [44]. The generalization of the results of several experiments, [39], gave the dependence (Fig. 2.11):

$$\Lambda/l_\sigma = 3.26\mathrm{Re}^{1/6}$$

The dependence satisfactorily generalizes data obtained under the intense evaporation (perfluorine-triethyl-amine) as well as under negligible evaporation (10% solution, T_0 = 8°C). So, probably, evaporation do not influence significantly on the critical wavelength. But till now no dedicated experimental neither theoretical investigation were devoted to such a problem.

Experimental study in [24] for the heating element with the size 2.22 × 68.05 mm^2 shows that the critical structure width is almost invariant with Re. Theoretical study in [24] predicts a slight monotonous decrease of Λ with increasing Re. It was found also that an increase of surface tension leads to an increase of the critical structure width. The law $\Lambda \sim \sigma^{0.365}$ was calculated for the 25 % alcohol water solution and Re = 0.51 that qualitatively in agreement with Fig. 2.11.

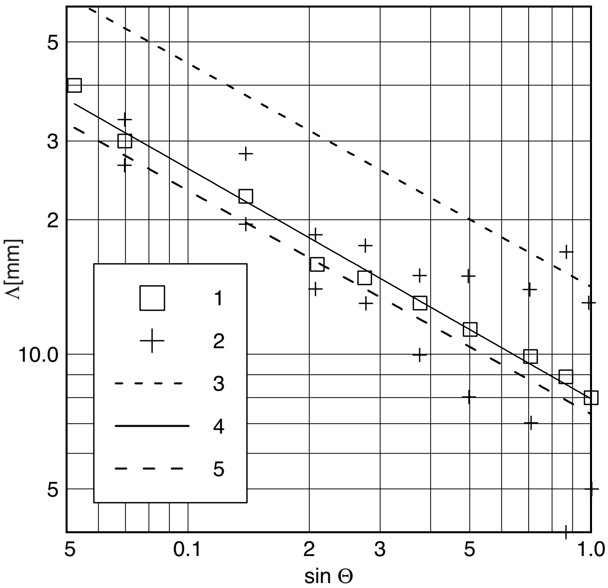

Figure 2.12. Dependence of regular structures wavelength on the plate inclination angle, [45], 10% ethyl alcohol mixture in water, Re = 1, T_0 = 20°C, heater 6.75 × 109 mm^2. 3- dependence $\Lambda/l_\sigma = 2\pi$ (critical wavelength for Rayleigh-Taylor instability [46, 47]), 4- average dependence for experimental data $\Lambda = 7.95(\sin\Theta)^{-0.52}$, 5- dependence $\Lambda/l_\sigma = 3.26\mathrm{Re}^{1/6}$.

The influence of plate inclination angle on the wavelength has been investigated in [45] for 10% ethyl alcohol mixture in water the heater size equal to 6.75 × 109 mm^2, Fig. 2.12. The angle of inclination with respect to the horizon has been varied from 3 to 90 degree. The results obtained at Re = 1 (T_0 = 20°C) are presented in Fig. 2.12. Significant increase of the wavelength has been revealed with the angle decreasing. At $\Theta = 3°$ the wavelength is equal to about 40 mm, i.e. by a factor 5 greater than the wavelength in case of the vertical plate which is equal to 8 mm. The obtained data has been generalized by the dependency

$$\Lambda = 7.95(\sin\Theta)^{-0.52},$$

where Λ has dimension of mm. Also, Fig. 2.12 shows maximum and minimum values of the wavelength measured in the experiment.

2.1.6. Supercritical Structure Width

The regular structures sharpen with increasing heat flux and its characteristic width (i.e. the distance between the rivulets) grows significantly, Fig. 2.13. Scale for the all pictures is the same. Also the upper edge of all images located in the same point on the liquid film. A shift of the structure upstream with more intensive heating at constant flow rate is visible.

A small jet between the main rivulets appears with increasing of heat flux, Fig. 2.13. Theoretical study in [23, 24] reveals that distinctive small rivulet in the centre of the structure appear due to a secondary thermocapillary instability of classical type [48] for nonzero heat flux at the free surface. Setting $\mathrm{Bi}_2 = 0$ leads to the disappearance of the small rivulet.

Measurement of the wavelength of the supercritical structures has been performed in [44] for perfluorine-triethyl-amine and heater 6.5 × 13 mm^2 at T_0 = 30°C. Experimental data are described by the dependency $\Lambda \sim q^{0.39}$. Structure width is changed from 3.37 mm to 4.76 mm when heat flux density is varied from 0.75 W/cm^2 to 1.79 W/cm^2. Experimental and theoretical study in [24] for the heating element with the size 2.22 × 68.05 mm^2 and 25 % ethyl alcohol mixture in water also shows that the supercritical structures width increase with increasing of heat flux. Comparison of Fig. 2.14 and Fig. 2.13a confirms again a small Re number effect on the critical structure width. Nevertheless, till now all details on dependency of the critical structure width on Re number and other parameters like surface tension, viscosity, size of the heater are not known. It should be emphasized that the results in Fig. 2.11 were obtained mostly for the heater 6.5 × 13 mm^2, which is short in the spanwise direction. As a rule, the whole structure consisted just of 3–4 horseshoe patterns, and therefore Λ could be essentially influenced by edge effects.

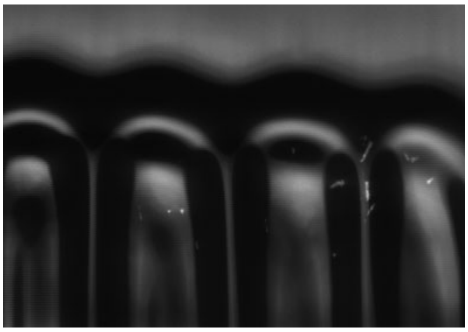

a) $q = q_{rol} = 2.4$ W/cm^2

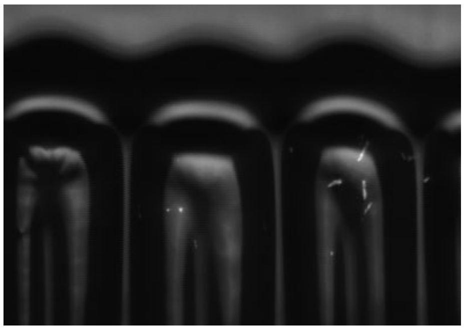

b) $q = 2.9$ W/cm^2

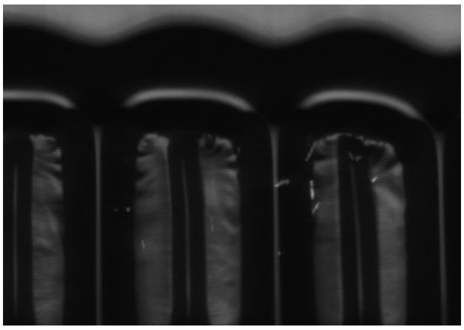

c) $q = 3.5$ W/cm^2

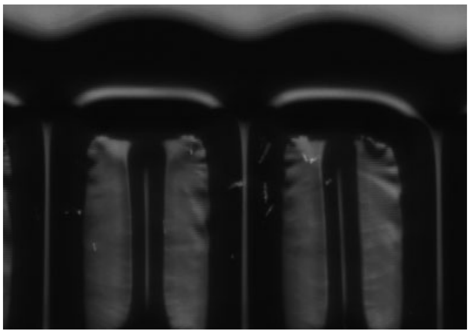

d) $q = 3.9$ W/cm^2

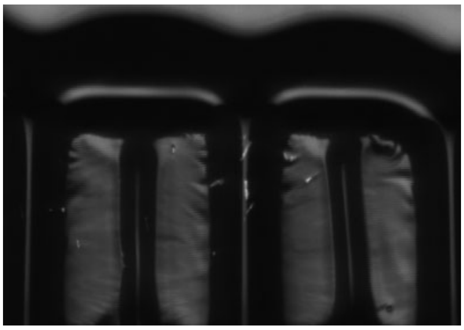

e) $q = 4.2$ W/cm^2

Figure 2.13. Supercritical structures, heater 6.7×68 mm^2, 25% ethyl alcohol in water, $T_0 = 20$°C, Re = 1, inclination angle = 90 degree, [39].

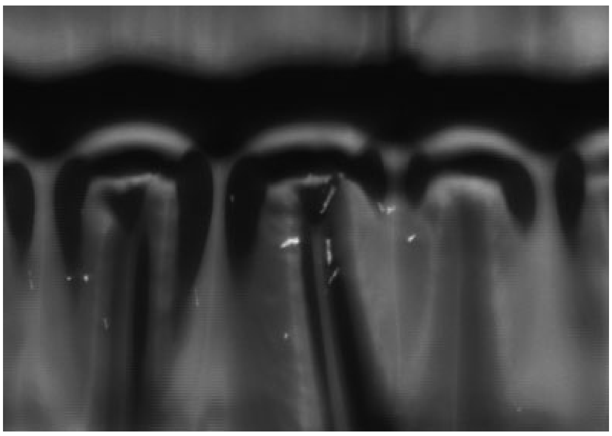

Figure 2.14. Slightly supercritical structures, heater 6.7×68 mm^2, 25% ethyl alcohol in water, $T_0 = 20$°C, Re = 0.091, $q = 0.63$ W/cm^2, inclination angle = 90 degree, [39].

2.2. Spatial Self-Organizing Structures at Moderate Re Numbers and Uniform Heating

2.2.1. Structures Formation

The other type of spatial self-organizing structures (an array of longitudinal rolls or rivulets and a thin film between them) was experimentally investigated in [49]. Rivulet formation in a water and dielectric fluid FC-72 film has been studied on a plate with a heater of 150 × 150 mm^2, i.e. at almost uniform heating. Condition of constant heat flux (q = const) is implemented on the heater surface. Nevertheless, heat redistribution takes place inside the heater that causes some heat flux non-uniformity. The Re number varies from 1 to 330. The initial temperature of the liquid is 17–28°C. The distance from the nozzle to the heater X_n is 41.5 mm and 120 mm. The setup is described in details in [50, 51] where self-organizing structures were also observed in liquid film of water.

Rivulet structures interact with hydrodynamical waves [8] that cause a complicated film flow patterns, Fig. 2.15. Structures sharpen at the end of the heater. Structure width, Λ, decreases from 20 mm to 15 mm for water with heat flux increasing that is opposite to the tendency described for regular structures at local heating (Fig. 2.13).

2.2.2. Temperature Field on the Surface of a Wavy Liquid Film

It is proven in [50, 51] by IR measurements that the instability has the thermocapillary nature. A detailed measurements of a temperature field on the surface of a wavy liquid film falling down a vertical plate with a heater of 150 × 150 mm^2 has been performed for water at the initial temperature T_0 = 20 °C using infrared camera COBA-2 in [52]. The registered range of IR radiation is 3.5–5.5 µm, and this allows receiving of main radiation from the liquid depth of about 10 µm. Frequency measurements was up to 164 Hz and uncertainty of measurement was estimated as ±0.25 °C.

Figure 2.16 shows an average infrared image of a liquid film. Strong temperature perturbations are seen in a spanwise direction. The highest surface temperature takes place in the thin film between rivulets. In Figs. 2.17 and 2.18 temperature of liquid film surface is measured along a one horizontal line. The scanning time for one line is 0.0061 seconds. In the upper part of the heater, X_t = 20 mm (X_t- distance from the upper edge of the heater), a hydrodynamic waves are dominated and in the lower part of the heater, X_t = 140 mm, thermocapillary effect changes the waves orientation to the vertical one.

A temperature evolution on the film surface during 1.2 seconds is shown in Fig. 2.19 for a distance 140 mm from the top edge of the heater. It is revealed that with an increase in the heat flux the temperature pulsations amplitude between the rivulets decreases that may be caused by the reduction

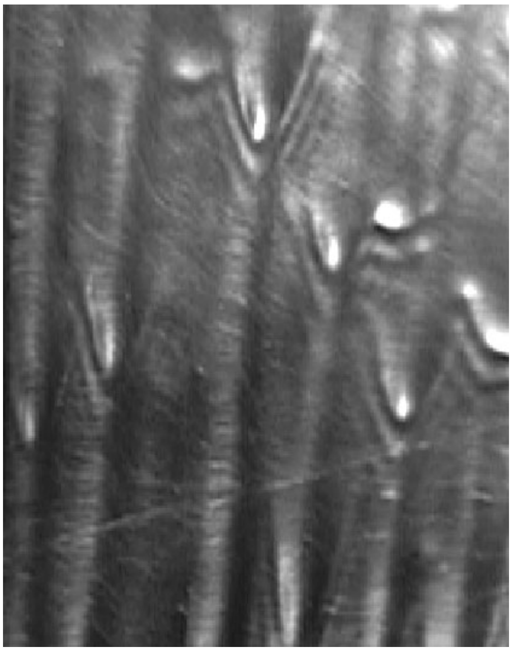

Figure 2.15. Rivulet structures interacting with hydrodynamic waves, Re = 22, q = 0.91 W/cm^2, water, T_0 = 24°C, [49].

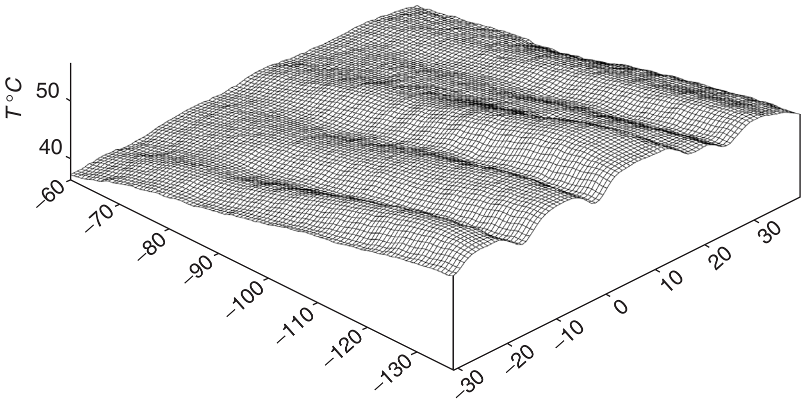

Figure 2.16. An infrared image of a liquid film, q = 1.23 W/cm^2, water, Re = 22, measurement rate - 1 frame per 1.2 second, [52].

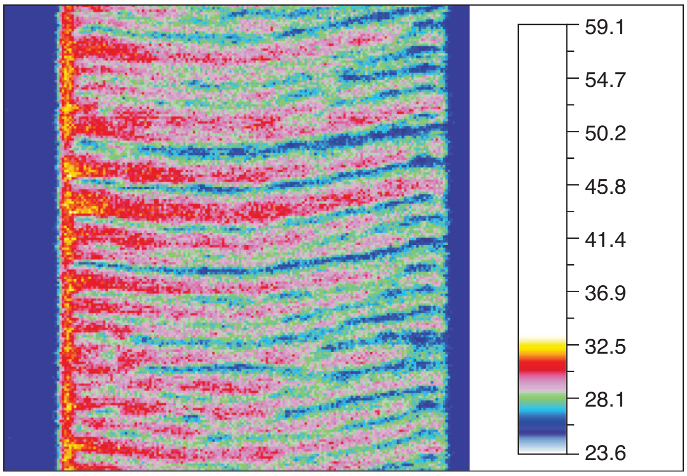

Figure 2.17. Temperature of liquid film surface, water, X_t = 20 mm, Re = 22, q = 1.3 W/cm^2, [52].

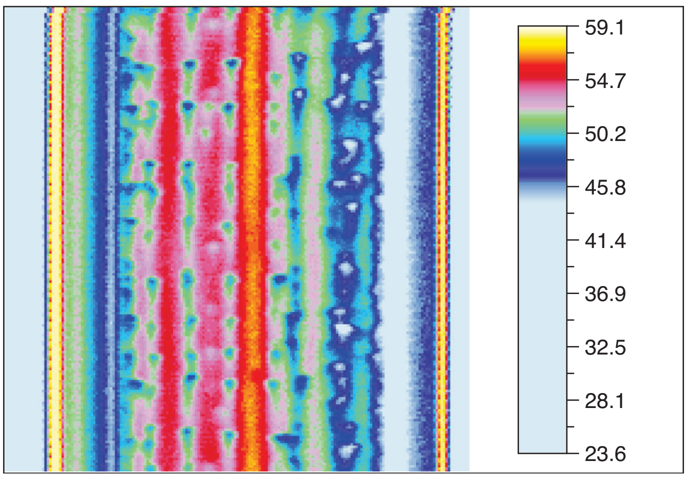

Figure 2.18. Temperature of liquid film surface, water, X_t = 140 mm, Re = 22, q = 1.3 W/cm^2, [52].

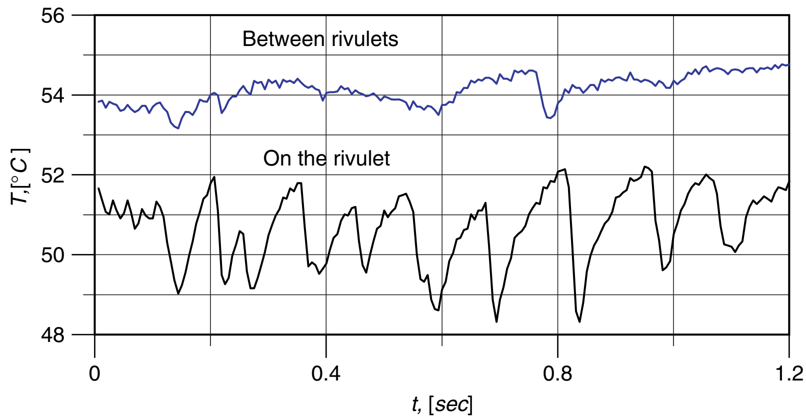

Figure 2.19. A temperature evolution on the film surface, [52].

of the local liquid flow rate. Contrary the temperature pulsations amplitude increases significantly on the crest of the rivulet (see also Fig. 2.18). Temperature pulsations up to 4°C are visible. A temperature difference between top of the rivulet and center of the trough can be more than 6°C.

The obtained results are in good qualitative agreement with the measurements of the local film thickness between the rivulets by the optical fiber probe [53]. It was revealed in [53] that with an increase of the heat flux the average film thickness, wave amplitude and thickness of the residual layer decreases.

2.2.3. Marangoni Effect on Wave Structure in Liquid Films

Capacitance and fluorescence techniques have been applied to measure local instantaneous film thickness on a heated substrate in [54]. Experiments have been performed with water film on a plate with a heater of 150×150 mm^2 at initial temperature of fluid equals to 20–24 °C and Re number varied from 15 to 40. Angles of the plate inclination to horizon (Θ) are varied from 15 to 90°. The distance from the nozzle to the heater X_n is 120 and 200 mm.

Eight capacitance sensors, mounted in one line, 6 mm higher than the lower edge of the heater are used. The distance between the sensors is equal to 2.5 mm, which significantly exceeds the size of the sensor (0.5 mm). To measure the phase velocity of the waves an additional single sensor is mounted at the distance of 12 mm upstream. Spatial resolution of the method is about 1 mm. The uncertainty of the measurement of the thickness of nonisothermal water film is less than 3%. The method is described in details in [55, 56].

Rhodamine 6Zh is used as a dye in fluorescence technique; it is not a surfactant and its fluorescent properties do not depend on temperature at low concentrations of solution. To excite phosphor a doubled NdYAG laser illuminating the surface area of 120×120 mm^2 on the plate is used. The light, re-radiated by phosphor, is registered by a digital PIV-camera with a red light filter operating under the mode of a double frame. Maximal frequency is equal to 7.5 Hz, spatial resolution is 0.1 mm and the accuracy of measurements is ±5–10 μm for the films with 200–400 μm thickness.

Wave structure in a liquid film is shown in Fig. 2.20 (Z is a coordinate across the film flow). A 40 mm width area in the central part of the heater is distinguished. A clear formation of rivulets for Re = 33 starts at $q = 0.64$ W/cm^2. With the heat flux increase the average film thickness at the rivulet increases and in the interrivulet zone decreases. The characteristic structure width Λ (i.e. the distance between rivulets) versus the inclination angle of substrate appear to depend on the plate inclination angle slightly. The dependence $\Lambda/l_\sigma = 4.3(sin\Theta)^{-0.04}$ is obtained that is quite different from the instability of regular structures at local heating, Fig. 2.12, and the instability of a "cold" capillary ridge [3].

Dependence of relative wave amplitude on the nondimensional heat flux is shown in Fig. 2.21 (q_b is the heat flux corresponding to the film rupture). Relative wave amplitude $A = ((h_{max})_{av} - (h_{min})_{av})/h_{av}$ is a ratio of the difference between the averaged values of maximal and minimal film thickness to the average value of film thickness in the area of measurements. Solid lines are the best linear low fit for the obtained results. Relative wave amplitude is increased slightly in the whole range of heat fluxes in the interrivulet area and is reduced in the rivulet. The transversal temperature gradients cause the film

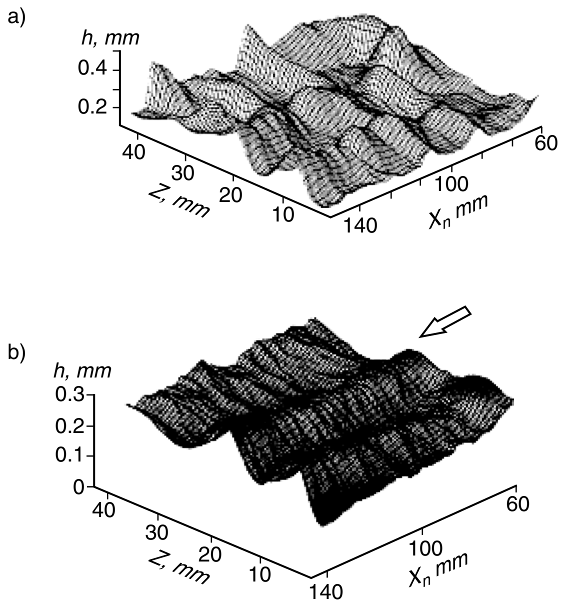

Figure 2.20. Liquid film distribution on a heated substrate (fluorescence technique), $q = 1.15$ W/cm^2 , Re = 33, $X_n = 200$ mm. Instantaneous (a); averaged by 30 measurements (b), [54].

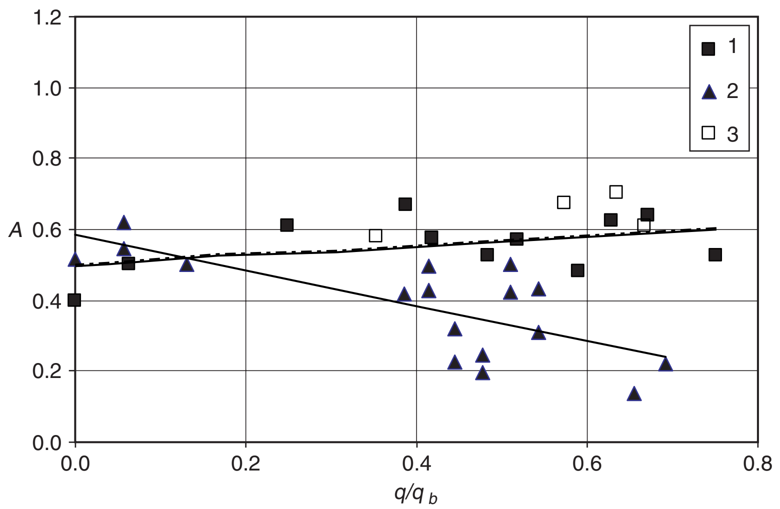

Figure 2.21. Relative wave amplitude versus nondimensional heat flux, Re = 33, X = 264 mm: 1 – interrivulet region, capacitance method, 2 – rivulet, capacitance method, 3 – interrivulet region, fluorescence technique, [54].

thickness reducing and the streamwise gradients cause growth of relative amplitude compare to the "cold" hydrodynamics (see also [57] for some details).

2.3. Film Rupture and Critical Heat Flux

2.3.1. Film Rupture

Dry patch formation in locally heated gravity driven films is preceded by formation of rivulet structures and their evolution [58]. The authors of [50, 59, 60] have reported that almost the same scenario of film rupture take place for the middle size heaters. Data for the heater size 150×150 mm^2 in a wide range of Re number (0.47–331) have been obtained. Dry spots usually appear at the bottom area of the heater and then spread to the upper part of the heater. As a result, a flow in the form of dry strips separated from each other by liquid rivulets is formed, Fig. 2.22. Hydrodynamic waves (variation of X_n) do not contribute significantly in the mechanism of film breakdown because film dynamics is controlled mainly by thermocapillary forces in the area where a first dry spot occurs.

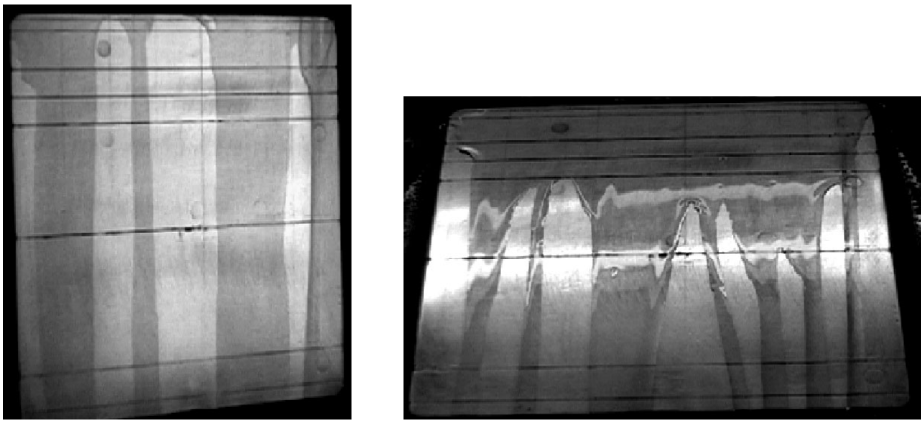

a) $Re_l = 1.119$, $q = 0.13$ W/cm^2 b) $Re_l = 2.62$, $q = 0.3$ W/cm^2

Figure 2.22. Flow of water film in the form of rivulets and dry strips, $Xn = 120$ mm, [59].

2.3.2. Critical Heat Flux for Film Rupture

It was shown in [58] that at Re = const the heat flux necessary for liquid film breakdown on local heaters is higher by two orders of magnitude than that on tubes 1–2 m height [61]. Subsequent investigations with local heating elements using dielectric liquid in [62] and "middle-sized" heater 150 × 150 mm^2 using water and 10% aqueous solution of ethanol [59] confirmed that heat flux, at which the film breakdown occurs, decreases significantly with increase of the streamwise heater length. Systematical investigations for various heaters and liquids have resulted in a correlation [63]:

$$K_p = 1932\,\mathrm{Re}^{0.66}\left[\frac{(\nu^2/g\sin\varphi)^{1/3}}{L}\right]^{0.90}\mathrm{Pr}^{-0.18}$$

where $Kp = -\,q_{idp}\,(\mathrm{d}\sigma/\mathrm{d}T)/(\lambda \cdot \rho \cdot (g \cdot \nu)^{2/3}$ is a ratio between the scale of thermocapillary tangential stress at the film surface and the scale of tangential stress at the wall in gravitational film flow. Parameters describing wave structure of the flow are not taken into account. Correlation is valid for the heater length and Reynolds number varying in the ranges of 2.2–150 mm and 0.3–226, respectively. Data for various liquid-solid systems are generalized by this expression in a wide range of the equilibrium wetting contact angles (from 11.4 to 43.5 degree).

Rupture of a subcooled liquid film flowing over a plate with a 150 × 150 mm^2 heater have been studied in [64] for high viscous liquids (ethylene glycol and aqueous solutions of glycerol) and plate inclination angle with respect to the horizon Θ changed from 3 to 90 degree. The threshold heat flux increases with the liquid viscosity. Criterion Kp was found to poorly generalize data for high viscous liquids. The criterion Kp was modified by taking into account characteristic critical film thickness $l_\delta = (l_\sigma^2\, l_\nu^3)^{1/5}$ for film rupture under isothermal conditions presented in [65]. The modified criterion has allowed to successfully generalize data for a whole range of studied μ, Re, Θ and q, by the equation (Fig. 1.23):

$$Kp(L/l_\delta) = 561Re^{0.72}\,.$$

2.3.3. Limit of Heat Flux for Gravity Driven Film

Many attempts of cooling of microelectronic equipment with falling films of liquid were done during the last decades. It was found that convective heat transfer and evaporation in thin liquid film ensures a sufficiently high heat transfer coefficient. Moreover, the pressure and temperature pulsations on the heat transfer surface, which are characteristic for liquid boiling are absent in case of falling films. Such semi-passive thermosyphon cooling systems may also provide a negligible hysteresis and moderate heat fluxes, while having minimal pump power requirements and being adaptable to three-dimensional packaging schemes.

The results of calculations of critical heat flux for dry patch formation using obtained correlations are shown in Figs. 2.24 and 2.25. Calculations have been done for two liquids, water and FC-72, and for moderate Reynolds numbers (Re ≤ 100). For size of electronic components in streamwise direction more than 2 mm the limit of critical heat flux that can be removed by gravity driven liquid film is equal

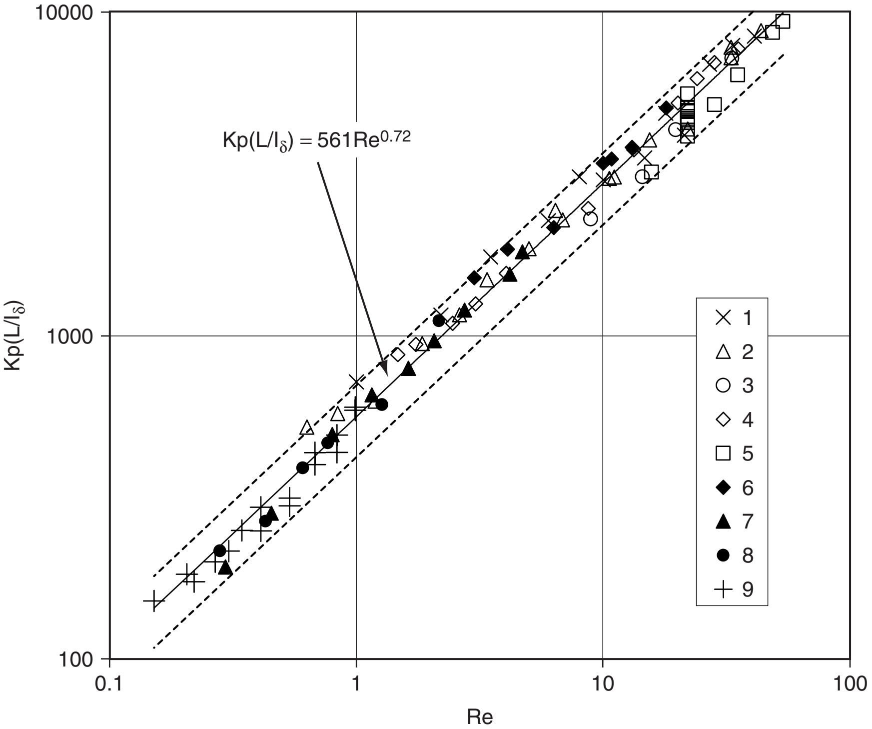

Figure 2.23. Data on threshold heat flux required for film rupture, $\Theta = 90$ deg, [64]: 1–4 – distilled water [59], 5 – distilled water [64], 6 – 10% aqueous solution of ethanol [59], 7, 8 – 50% and 60% aqueous solution of glycerol, respectively [64]; 9 - ethylene glycol [64]. Data [59] were obtained at $T_0 = 20$–25°C, $X_n = 41.5$–200 mm. Solid line – generalization of all the data. Dashed lines indicate interval of ±25%.

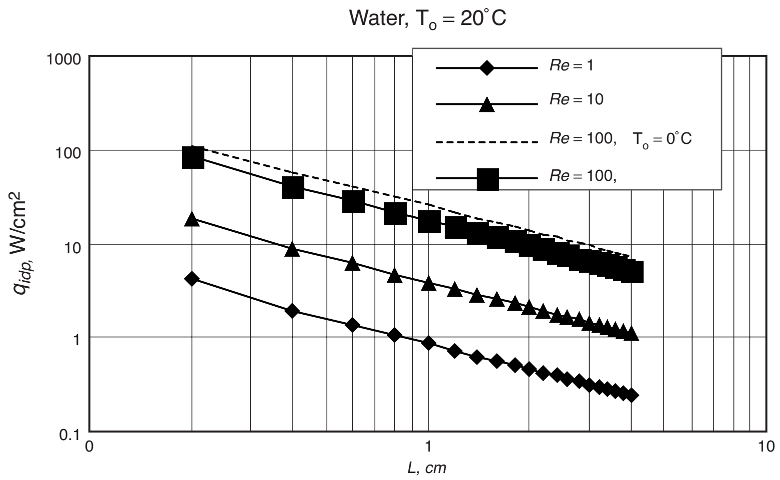

Figure 2.24. Critical heat flux for dry patch formation in water liquid film depending on heater length and *Re* number.

to 100 W/cm^2 for water ($T_0 = 20$°C) and 10 W/cm^2 for FC-72. Decrease of the initial liquid temperature slightly increases this value.

It should be noted that correlation has been obtained for heating elements with smooth surface and for low intensity of evaporation. According to the knowledge of the author, the data for evaporation effect and surface topology effect are very limited in the literature for small size heaters. Some details concerning investigations of rupture of falling films can be found in [66, 67, 68, 69, 70, 71, 72]. Correlation has been obtained for the width of the heating element large enough compare with the characteristic structure width, $B_h \gg \Lambda$. The data for the heater width effect is very limited in the literature for small size heaters.

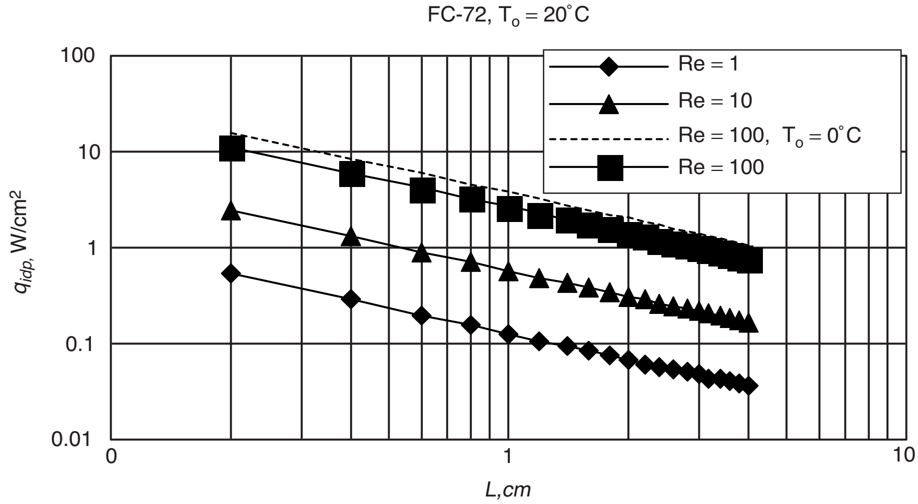

Figure 2.25. Critical heat flux for dry patch formation in FC-72 liquid film depending on heater length and *Re* number.

3. SHEAR-DRIVEN LIQUID FILMS AT LOCAL HEATING

3.1. Two-Phase Flow and Heat Transfer in Microchannels

The flow of vapor and liquid in a channel can take various forms depending on the distribution and extent of "aggregation" of the two phases, with each distinct vapor/liquid distribution referred to as a "flow regime." Four primary two-phase flow regimes: Bubble, Intermittent, Annular, and Stratified, as well as numerous sub-regimes, have been identified in the literature [73, 74]. Bubbly flow is associated with a uniform or non-uniform distribution of small spherical or non-spherical bubbles within the liquid phase. Intermittent flow is characterized by the flow of liquid "plugs" separated by elongated gas bubbles – often in the shape of "slugs" or bullets – though sometimes more chaotically mixed. In Annular flow, a relatively thin liquid layer flows along the channel walls, while the vapor flows in the center of the channel, creating a vapor "core" which may also contain entrained droplets. In vertical channels with heat addition, where the vapor content increases in the flow direction the Bubbly regime is followed sequentially by the Intermittent and Annular regimes.

Referring to the review papers [30, 75], the experimental two-phase heat transfer coefficients obtained in the studies [76, 77] provides clear evidence of a possible M-shaped variation of heat transfer coefficient with thermodynamic quality. The empirical heat transfer coefficients rise steeply from the values attained for slightly subcooled conditions to a local maximum at a near-zero quality, after which the heat transfer coefficient values fall with higher quality towards a plateau-like region, only to reach another inflection point at moderate qualities (15%–40%), where the curve once again attains a positive slope. Beyond this point, the heat transfer coefficient rises with increasing quality until it reaches a second local peak, at elevated quality values, of approximately 50% [76] and 75% [77]. For even higher vapor qualities, the heat transfer coefficient deteriorates until reaching the minimum reported values, at qualities approaching unity, generally associated with observed dryout conditions.

While sub-micron liquid films offer great promise for the thermal management of high flux electronic components, the current literature reveals that deep into the annular regime, but at qualities well below those required to form such thin films, a steep decrease in heat transfer occurs. The classical macro-pipe two-phase heat transfer correlations have been found to provide good agreement with the low-quality annular flow data [30, 75], but the thermodynamic quality at which partial dryout occurs and the ensuing steep decline in the heat transfer coefficient are not predictable by the available macro-pipe correlations.

3.2. Experimental Setup

Figure 3.1 shows design of the typical test section. The main part of the test section is a stainless steel plate with a flush-mounted copper rod. At the working surface the rod has a 1×1 cm^2 head emulating surface of a computer chip. Construction of the heater provides the condition at the heater surface $T =$

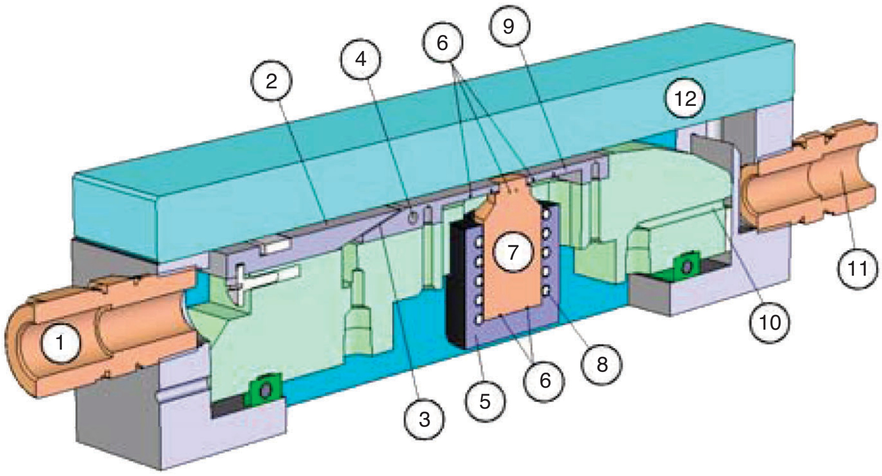

Figure 3.1. Design of test section [37, 78, 79]. 1- gas inlet; 2- channel; 3- liquid nozzle; 4- thermostabilizer; 5- heat insulation (mineral wool); 6- thermocouples; 7- copper rod; 8- Nichrome spiral; 9- stainless steel plate; 10- liquid outlet; 11- gas outlet; 12 – glass cover.

const (which is confirmed by three thermocouples measurements). The test section is covered with a transparent cover made of optical glass so that a flat channel with variable height (0.2...2 mm) is formed.

Distilled water with initial temperature of about 24°C or dielectric fluid FC-72 are used as the working liquids. Air with temperature of 24–27 °C and relative humidity of 15–30% or dry nitrogen are used as the working gases. The experiments are carried under atmospheric pressure. The test section is set horizontally. When investigating liquid films falling under the action of gravity the test section is set vertically while the glass cover is removed. Gas, pumped by a compressor, flows through the channel and passes to the atmosphere. Gas flow rate is measured by a Bronkhorst digital thermal mass flow meter. Liquid, supplied from a thermostat, gets into the channel through a liquid nozzle and flows under the friction of the gas along the stainless steel plate as a film. The liquid rate is measured by a float-type rotameter or a syringe pump.

Distance from the gas inlet to the liquid nozzle is 57 mm while distance from the liquid nozzle to the heater is 32 mm. This provides steady flows of gas and liquid at the moment they reach the heater. Channel width is 30–40 mm. Several thermocouples are embedded in the stainless steel plate and in the copper rod, allowing determination of the working surface temperature. The temperature of the heater surface is calculated taking into account the depth at which the thermocouples are embedded (2 mm). All the thermocouples are individually calibrated to an accuracy of 0.1°C. The heat flux is determined by the electrical power dissipated on the heating spiral. Thermal conductivity of copper is 400 W/mK which is almost 30 times higher than that of stainless steel (15 W/mK). This provides heat spreading to the stainless steel plate of about 10% at $q > 250$ W/cm^2, of about 20% at $q = 100$ W/cm^2 and of up to 30% for smaller heat fluxes (according to the measurements by thermocouples embedded into the substrate) [79].

3.3. Flow Sub-Regimes in Pseudo-Stratified Flow (Water)

A study of two-phase flow regimes in the short (length of 80 mm) rectangular horizontal channel in the wide range of gas and liquid flow rates has been made in [80, 81, 82, 83] for the channel height varied from 200 µm to 1 mm. Schliren and Laser Induced Fluorescence techniques have been used for registration of time-dependent liquid flow. New flow regimes (jet and bubble-jet) have been detected. It was shown that the instability of liquid flow near the sidewalls influents essentially on the transition between several regimes. A region of the Separate Flow regime decreases with the channel height, but in contrast to the case of cylindrical tubes [84], this region does not vanish, at list for 200-µm-thick channels.

A detailed experimental investigation of a shear-driven film of water (Pseudo-Stratified flow) was undertaken in [34], Figs. 2.2 and 2.3. The test section was set horizontally and the heater of 22 × 6.55 mm size was embedded into a thermostabilizing copper block. The channel height was 2 mm and the film flow width W_f varied from 65 to 120 mm. Adiabatic flow (all heaters switched off) was investigated in the range of $Re_l = 1–60$ and $Re_g = 60–1950$. Initial temperature of the liquid was 20–22 °C.

The experiments revealed the existence of three sub-regimes in this stratified flow configuration – smooth film flow, film flow with 2D waves, film flow with 3D waves. It was found that a liquid film of water driven by the action of a gas flow in a channel is stable (no any deformations on the gas-liquid interface were detected) in a wide range of liquid/gas flow rates, Fig. 3.2. At relatively small Re_l and relatively high Re_g the film ruptures. For a narrower flow the film is considerably more stable against rupture than for a wider flow. At relatively high Re_l and relatively small Re_g the film thickness increases and can result in part of the channel flooding. Inverted flow takes place in this case, i.e. a rivulet of gas is moving on the upper glass plate. With increasing Re_l and Re_g, first, two dimensional (2D) waves form at the film surface and then they break into three dimensional (3D) ones. The Kelvin-Helmholtz instability can be the main reason for such wave formation [8].

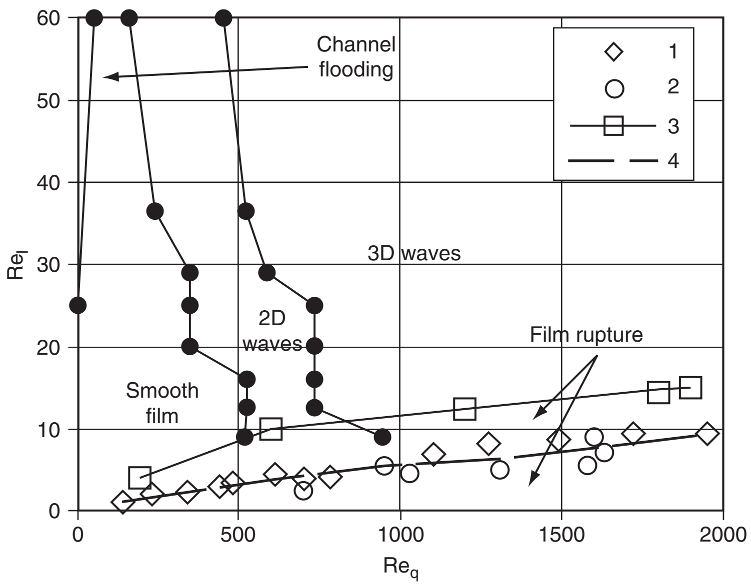

Figure 3.2. Map of adiabatic flow regimes. Film rupture: 1, 2- W_f = 65 mm, run 1 and 2, respectively; 3- W_f = 120 mm; 4- generalization of data 1, 2. All the rest data - W_f = 65 mm, [34].

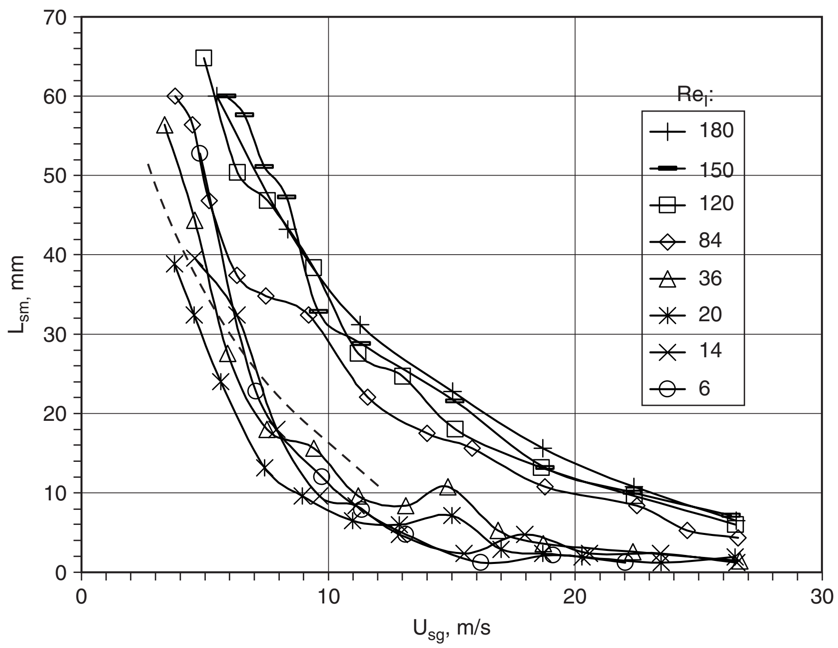

Figure 3.3. Length of smooth region in the film, depending on superficial gas velocity for different liquid Re numbers, H=1.5 mm [79]. Dashed curve – data [34] for Re_l=9-29, H = 2 mm.

Figure 3.3 presents influence of Re_l and U_{Sg} on the length from the liquid nozzle to the beginning of the wave formation, i.e. the length of smooth region, L_{sm} [79]. Statistical error in determining L_{sm} is about ±3 mm. In general, L_{sm} decreases with increasing U_{Sg} and with decreasing Re_l. However for $6 \leq Re_l \leq 36$ and $120 \leq Re_l \leq 180$ L_{sm} is practically independent on Re_l (within the limits of experimental error). This is consistent with [34] where Re_l was found to have little or no effect on L_{sm} in the range $9 \leq Re_l \leq 29$. As it is seen from Fig. 3.3, data on L_{sm} from [34] correlates well with the data in [79].

3.4. Rupture of Shear-Driven Liquid Film (Water)

Rupture of shear-driven liquid film was investigated in [34, 37] in the range of the average heat flux $q = 0.87$–32.1 W/cm^2, which was determined by the electric power dissipated on the heater. Parameters of the experiment are $Re_l = 5.5$–36.5, $Re_g = 160$–1480. The scenario of film rupture is different for different flow sub-regimes. In the smooth film sub-regime, the increase of the heat flux first causes a faintly visible deformation of the film surface at the bottom edge of the heater and then the film suddenly ruptures, with virtually instant dryout of the whole heating area.

In the sub-regime of 2D waves, rupture is preceded by formation in the film of an unstable hollow at the bottom part of the heater, periodically enhanced by the passage of 2D waves. The first stable dry patch forms at the bottom edge of the heater at some threshold heat flux and slowly increases in size with time. With further increase of the heat flux it completely covers the heater. In the sub-regime of 3D waves, the increase of the heat flux leads to formation of an unstable 3D structure, heavily altered by the passing 3D waves. With increase of the heat flux, usually two dry patches form at the bottom edge of the heater, making the 3D structure more stable.

Figure 3.4 shows the threshold heat flux at which an initial stable dry patch forms, q_{idp} depending on Re_l and Re_g. It is seen that q_{idp} increases with increasing both Re_l and Re_g. Dashed lines represent previously obtained data on rupture of a water film falling down a vertical plate with a heater of 13 × 6.5 mm (similar length) [58]. At relatively small Re_l the shear-driven liquid film breaks down at similar or even lower heat fluxes compared to gravity-driven one. However at higher liquid Re number q_{idp} for shear-driven liquid film is by a factor 3 higher.

3.5. Flow Sub-Regimes in Rectangular Channel (FC-72)

The scheme of the test section for experiments with FC-72 shear-driven liquid film is shown in Fig. 3.5. It is almost similar to the test section depicted in Fig. 3.1. The basic element of the test section is a flat plate made of copper having dimensions of 135 × 60 × 10 mm in length, width and depth, respectively.

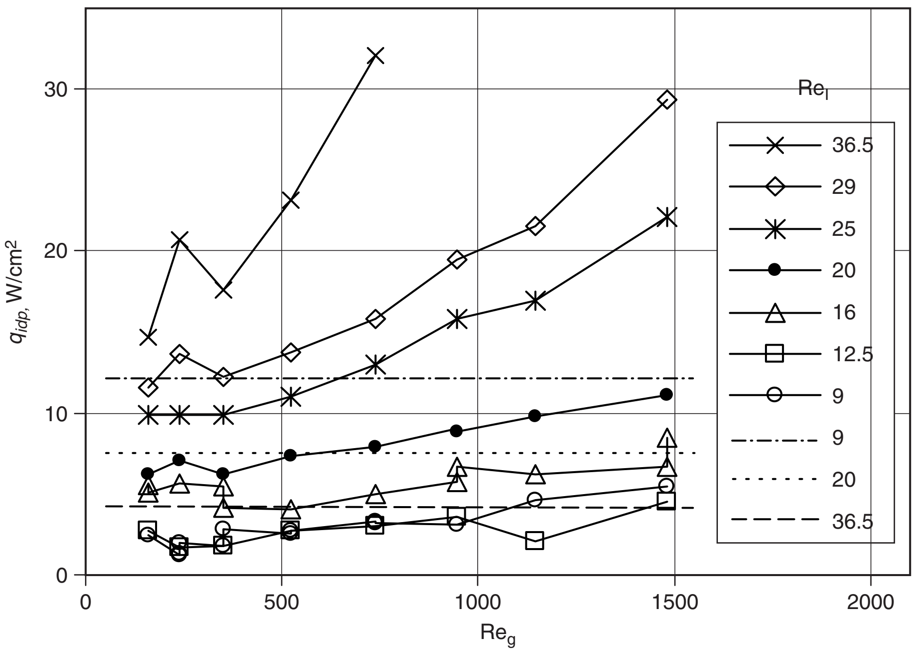

Figure 3.4. Threshold heat flux for film rupture [37], dashed lines – data on a falling water film [58].

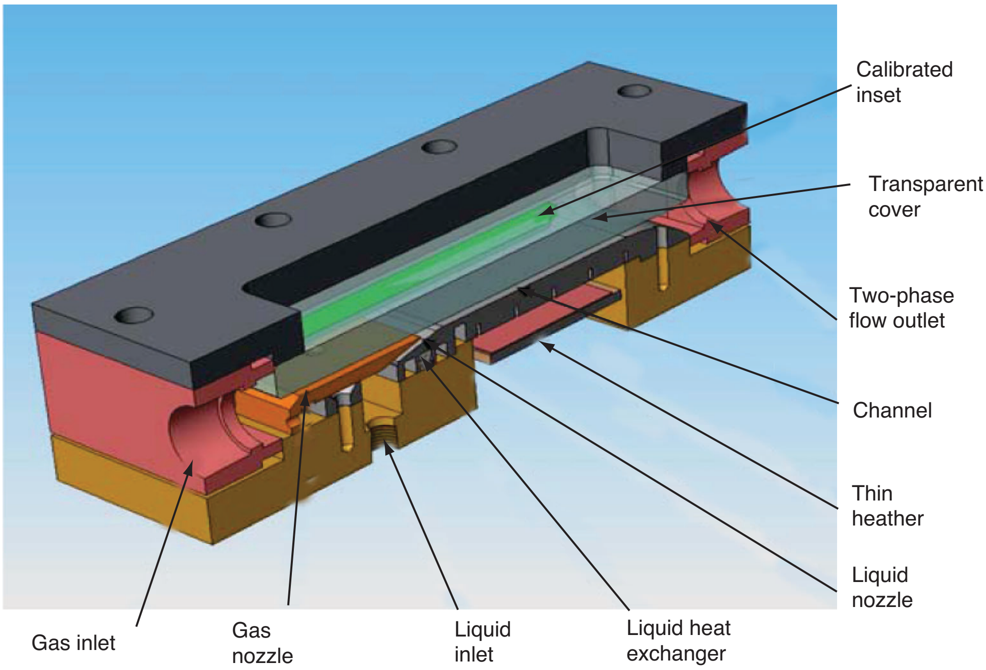

Figure 3.5. Scheme of the test section with a constant temperature boundary condition on substrate.

This plate is placed on the support made of textolite. The plate is covered with a transparent, glass cover so that a channel of variable height can be created. Dimensions of the channel in the present experiment (height×width×length) are 2 × 40 × 80 mm. The bottom of the channel has been polished to a mirror surface. Controlled by syringe pump, FC-72 is supplied from a liquid container into a buffer chamber and a nozzle of variable height. Dry nitrogen gas is supplied from a balloon.

Flow visualization by Phase Shifting Schliren technique (PSS) has been used. Adiabatic flow is investigated in the range of Re_l = 4–32 and Re_g = 15–2100. Figure 3.6 shows the obtained flow sub-regime map. In the present experiment PSS has been used like conventional Schliren system. The system has provided a possibility to use vertical and horizontal orientation of the "knife", which

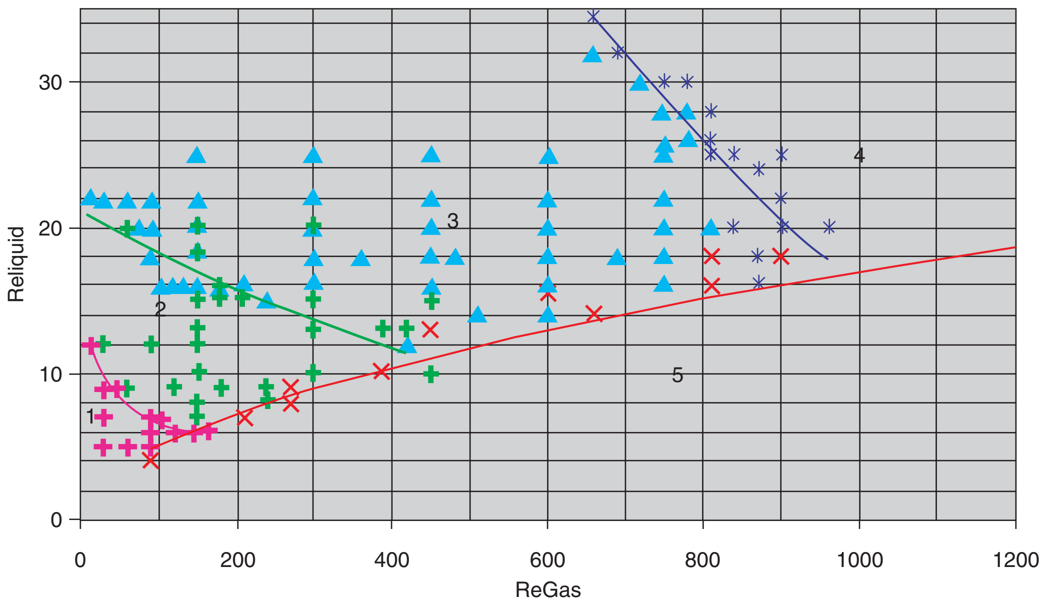

Figure 3.6. Adiabatic flow sub-regime map, FC-72- Nitrogen, T_0 = 20°C, [86]: 1- Ripples, 2-Structures, 3- 2D waves, 4- 3D waves, 5-film rupture.

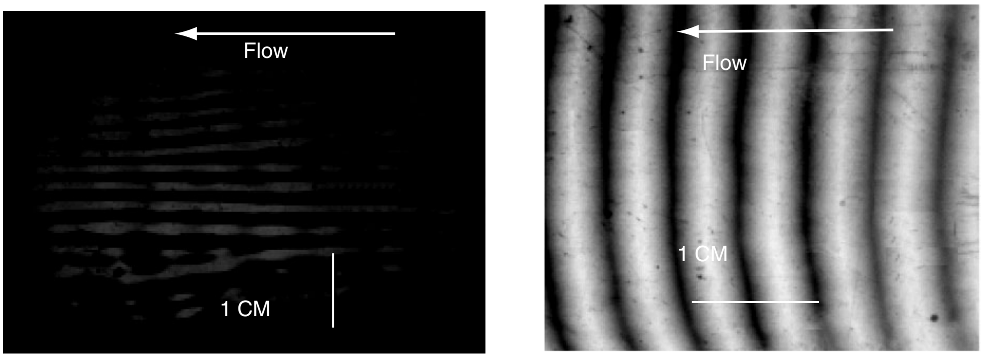

a) Structures b) 2D waves

Figure 3.7. 2D waves flow regime with structures, $Re_l = 18$, $Re_g = 600$, [86].

corresponds to measurements of the gas-liquid interface deformations in the streamwise and spanwise directions, respectively [85], Fig. 3.7.

For small liquid and gas flow rates the weak deformations ("Ripples" and "Structures") are visible on the gas-liquid interface, Fig. 3.6. In the "Ripples" sub-regime streamwise size of the cells is approximately equal to the distance between two structures. With increasing gas Reynolds number, the "Ripples" sub-regime is transformed into the "Structures" sub-regime. With increasing Re_l and Re_g, first two dimensional waves form (sub-regime-3) at the film surface and then they break into three dimensional ones (sub-regime-4). Two-dimensional and three-dimensional waves are usually observed with structures. Figure 3.7 shows a vertical and horizontal Schliren image for the same flow parameters. Rupture of the liquid film (sub-regime-5) has been observed for all tested Re_l at some fixed Re_g. It was identified that highly volatile liquid film of FC-72 driven by the action of a gas flow in a mini-channel is unstable for all liquid/gas flow rates.

3.6. Critical Heat Flux for Shear-Driven Liquid Film

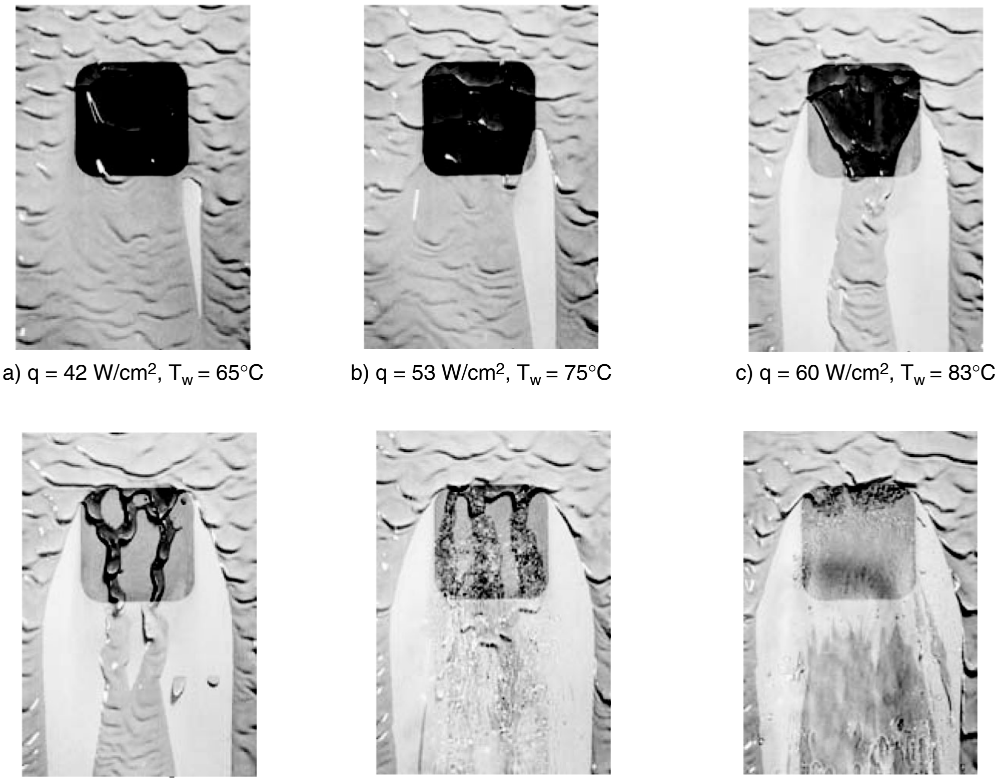

a) $q = 42$ W/cm^2, $T_w = 65$°C b) $q = 53$ W/cm^2, $T_w = 75$°C c) $q = 60$ W/cm^2, $T_w = 83$°C

d) $q = 79$ W/cm^2, $T_w = 108$°C e) $q = 159$ W/cm^2, $T_w = 128$°C f) q=201 W/cm^2, crisis

Figure 3.8. Film rupture and crisis in a shear-driven liquid film, $Re_l = 21.1$, $Re_g = 2150$, flow directed from top to bottom [78].

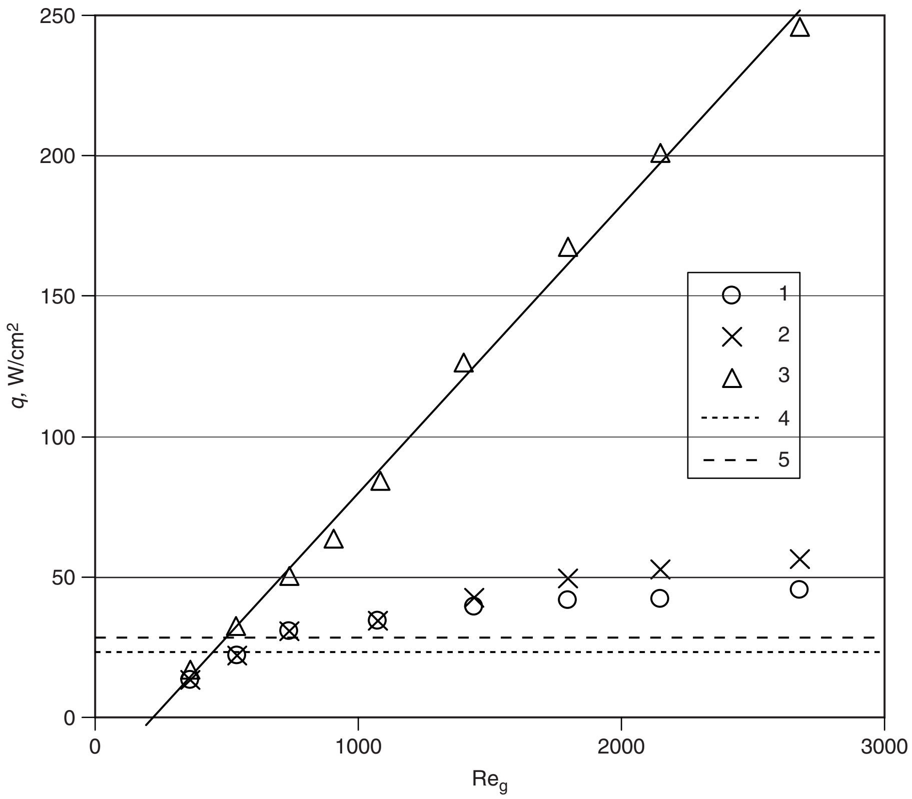

Figure 3.9. Effect of gas flow on film rupture and crisis, Re_l = 21.1, [78]. 1- q_{idp} (Fig. 2.8a); 2- q_{idp} on the heater (Fig. 2.8b); 3- CHF (Fig. 2.8f); 4- q_{idp} for a falling liquid film (vertical plate, no gas); 5- CHF for a falling liquid film.

The test section depicted in Fig. 3.1 has been used for the measurements. Figure 3.8 presents pictures of film rupture and crisis in shear-driven liquid film at Re_l = 21.1 and Re_g = 2150. From Fig. 3.8a it follows that even for sufficiently high gas flow rate (Re_g = 2150) an important thermocapillary effect on film dynamics take place. Initial dry patch forms along the heater side boundary several millimeters lower the bottom edge of the heater, i.e. in the area where thermocapillary forces acting in spanwise direction decrease the film thickness.

Figure 3.9 shows the effect of gas flow rate on the threshold heat flux for film rupture and on CHF (critical heat flux) for a shear-driven liquid film in comparison with a falling liquid film. At relatively small Re_g the shear-driven liquid film is less stable to rupture and to crisis occurrence in comparison with falling liquid film. However at higher gas Reynolds numbers q_{idp} for shear-driven liquid film is up to 2 times higher, while CHF, linearly growing with Re_g, is up to 10 times higher than CHF for falling liquid film and reaches value equal to 250 W/cm^2.

For a gravity-driven liquid film the threshold heat flux for film rupture and the critical heat flux are close: CHF is about 20% higher than q_{idp}. For a gas shear-driven liquid film with an increase of Re_g inertial force starts to dominate acting against thermocapillary forces, which provides more uniform liquid distribution over the heater as compared to a gravity-driven liquid film. As a result, CHF for a gas shear-driven liquid film may be higher than q_{idp} by a factor 5.

The high heat fluxes achieved makes use of shear-driven liquid films promising for cooling applications. Since the experiment was performed at atmospheric pressure, sufficiently high wall temperatures take place (up to T_w = 133°C at Re_g = 2700). High temperature is needed to ensure intensive evaporation. It is evident that decreasing pressure in the system will allow decreasing the heater temperature, what is needed for microelectronics cooling.

4. MATHEMATICAL MODELLING OF SHEAR-DRIVEN LIQUID FILM AT LOCAL HEATENG

A 2D steady mathematical model for a locally heated incompressible liquid film that is moving in the channel under the influence of the gas flow as well as under gravity force have been studied recently in [33, 35, 87, 88]. Numerical and analytical calculations for horizontal mini-channels have been performed. In [88] for steady laminar flow of liquid film and co-current gas in a channel analytical solution of problem of temperature distribution for linear velocity profile has been obtained. In [33] calculations have been performed for steady laminar flow of liquid film and co-current gas flow in plane channel with the height varied from 150 to 500 μm, temperature dependent viscosity and an influence of liquid film deformations on pressure and velocity in a gas phase were taken into account. In [35, 87, 89] an investigation of the evaporation effect on the heat transfer of liquid film flow in a channel has been performed. In [36] a 3D time-dependent model has been elaborated.

4.1. Problem Statement

We consider a flow of non-isothermal thin film of viscous incompressible liquid forced by co-current gas flow, in a horizontal mini-channel. A Cartesian coordinate system (x, y, z) is chosen such that the axis Ox is directed along the liquid flow. The liquid occupies a domain:$\{(x, y, z): -\infty < x, y < \infty, 0 < z < H(t, x, y)\}$. The mathematical statement of the problem under consideration is described in details in [36]. For more details also see [90, 91, 92, 93, 94]. 3D time dependent mathematical model of joint laminar motion of a thin liquid film and co-current gas, which creates the tangential force on the gas-liquid interface, in a flat minichannel with a local heater is used. The liquid motion is described by the Navier-Stokes, continuity and energy equations. At the substrate the no-slip condition is imposed together with the thermal boundary condition $kT_z = -q$. A given heat flux density q on the heater and heat insulation condition before and behind the heater is used. At the free surface (at $z = H$) boundary conditions are supposed to be as follows:

$$H_t + (\bar{\mathbf{v}} \cdot \nabla)H - w = 0, \tag{1}$$

$$k\,\partial T/\partial n + b_2(T - T_2) = 0, \tag{2}$$

$$(p_0 - p)\vec{n} + 2\mu\bar{\mathbf{D}} \cdot \vec{n} = \sigma K\vec{n} + \nabla_s\sigma + \vec{\tau}, \tag{3}$$

Here $\nabla_s = \nabla - \vec{n}(\vec{n} \cdot \nabla)$ - surface gradient, $\sigma = \sigma_0 - \gamma\,(T - T_0)$, where $\gamma = -\sigma_T = \text{const} > 0$. Case $b_2 > 0$ corresponds to the cooling of the liquid. Effects of surface tension, temperature dependent viscosity, thermocapillarity and gravity are taken into account.

The initial parameters such as the film thickness H_0, tangential stresses and the pressure drop are found out as the solution of the problem of isothermal laminar co-current flow in the channel - Couette flow with nonzero pressure drop [36]. The tangential stress is expressed as follows:

$$\tau = \mu_g \left(-\frac{\lambda H_0}{\mu_g} + \frac{A_1\mu H_0{}^2 + A_2\mu(d^2 - H_0^2)}{2\left[\mu(d - H_0) + \mu_g H_0\right]} - \frac{2(A_1\mu - A_2\mu_g)H_0{}^2}{2\left[\mu(d - H_0) + \mu_g H_0\right]} \right). \tag{4}$$

where $A_1 = \dfrac{\lambda + \rho g \sin\alpha}{\mu}$, $A_2 = \dfrac{\lambda}{\mu_g}$. Liquid pressure is supposed to be equal to $p = p_0 - \lambda x + \rho g z \cos\alpha$. λ = const is proportional to the gas Reynolds number (Re_g). It is supposed in the present problem that there is no influence of liquid on the gas flow. The gas influence on a liquid film is determined in occurrence with a constant tangential stress on the free surface, a pressure gradient along the flow and Biot number at the interface.

Performing a change of variables $\xi = z/H$, $u^1 = uH$, $v^1 = vH$, $w^1 = w - u\xi H_x - v\xi H_y$, we rewrite the governing equations and the boundary conditions in the layer $0 < \xi < 1$, $-\infty < x, y < \infty$. Assuming the long-wave approximation to be valid in terms of the small parameter $\varepsilon = H_0/l \ll 1$ the system is rewritten in a non-dimensional form with the dimensionless criteria defined as:

$$A = \frac{g\sin\alpha H_0^3}{U^2 l^2} + \frac{\lambda}{\rho U^2},\ C = \frac{g{H_0}^2\cos\alpha}{U^2 l} = \frac{\cos\alpha}{Fr},$$
$$Ma = \frac{\sigma_T Q H_0^2}{\mu_0 U l},\ D = \frac{H_0\mu_0 c_p}{lk} = \varepsilon\,\mathrm{Pr}, Bi_2 = \frac{b_2 H_0}{k}.$$

The scales for temperature, velocity and streamwise length are respectively:

$$Q = \sup_{t,x,y}\frac{q}{k},\ U = \frac{\mu_0}{\rho H_0},\ l = \left(\frac{\sigma_0 H_0^2}{\rho U^2}\right)^{1/3}.\ \text{where}\ \ \mu_0 = \mu(T_0).$$

The resulting evolution equation for the film thickness is

$$h_t + \left[h^3\varphi(\Delta h - Ah + Cx)_x + Ma\ h^2\gamma\tilde{\theta}_x - h^2\gamma\hat{\tau}\right]_x + \left[h^3\varphi(\Delta h - Ah)_y + Ma\ h^2\gamma\tilde{\theta}_y\right]_y = 0. \tag{5}$$

And the equation for the dimensionless temperature θ is obtained as

$$Dh\left[h\theta_t + u\theta_x + v\theta_y + \left(w - \xi w|_{\xi=1}\right)\theta_\xi\right] = \varepsilon^2 h^2\Delta\theta + \left[1 + \varepsilon^2\xi^2\left(h_x^2 + h_y^2\right)\right]\theta_{\xi\xi} - 2\xi\varepsilon^2 h\left(h_x\theta_{x\xi} + h_y\theta_{y\xi}\right) + \varepsilon^2\xi^2\left[2\left(h_x^2 + h_y^2\right) - h\Delta h\right]\theta_\xi. \tag{6}$$

Finally, it remains two unknown field variables $\theta(t, x, y, \xi)$ and $h(t, x, y)$, defined by the system of Eqs. (5) and (6). The energy equation is solved in a nonsimplified form, because convection and conduction are equally essential for heat transfer at intensive local heating. It is supposed also that for the local heating of the film at initial time moment temperature distribution is uniform and film is not disturbed and that far from the place of the localized heating all disturbances decay. Additional initial and boundary conditions are as follows:

$$\begin{aligned} &\theta|_{t=0} = 0;\quad \theta \to 0\ \ at\ x, y \to \pm\infty, \\ &h|_{t=0} = 1;\quad h \to 1, h_x \to 0\ \ at\ x \to \pm\infty, \\ &h \to 1, h_y \to 0\ \ at\ y \to \pm\infty. \end{aligned} \tag{7}$$

4.2. Numerical Scheme

Solution of the Eqs. (5), (6) with corresponding conditions is implemented as follows. It is assumed that the centre of the heater is located in the origin of coordinates. X axis is oriented along the gas flow. The solution of the problem in unlimited on x,y area is changed to solution in the field $\{x \in (-x_1, x_2), y \in (-y_1, y_2)\}$. The initial conditions and conditions of the heat balance save their form but the boundary conditions are transformed as follows:

$$\begin{aligned} &h_x\big|_{x=-x_1} = h_y\big|_{y=-y_1} = h_y\big|_{y=y_2} = h_x\big|_{x=x_2} = 0, \\ &h|_{x=-x_1} = h|_{y=-y_1} = h|_{y=y_2} = 1,\ \theta|_{x=-x_1} = \theta|_{y=-y_1} = 0, \\ &\theta|_{y=y_2} = 0, h_{xx}\big|_{x=x_2} = 0,\ \theta_x\big|_{x=x_2} = 0. \end{aligned} \tag{8}$$

Since value of functions θ and h are unknown on boundary $x = x_2$ the corresponding boundary conditions are replaced by "soft" one. The problem of heat transfer and the equation for the gas-liquid interface deformation are solved by the finite difference method. The splitting method by introducing fractional steps is used. And each of new difference equation was solved by the sweep method.

Calculations are carried out under the following conditions. Material constants correspond to a liquid FC-72 driven by the Nitrogen gas flow in a horizontal minichannel (i.e. inclination angle α is equal to 0°) at $T_0 = 20°C$ [36]. It is assumed that substrate is heat-insulated, i.e. heating intensity is equal to zero on the substrate, excluding heater region, where heating intensity is constant and equal to q, i.e. $T_2 = T_0$.

When calculations are carried out for FC-72, the liquid with low value of heat capacity, assumption that free surface is heat-insulated is not realistic, it leads to a significant liquid overheat [36]. Heat dissipation at the free surface become important and should be taken into account for example by using Biot number Bi_2. In addition FC-72 is a low boiling liquid that leads to noticeable evaporation even at low gas velocity and temperature (about 20 °C). Using of Newton low as the boundary condition at the gas-liquid interface allows us to model qualitatively the effect of evaporation. Especially this assumption is valid when evaporation does not change the liquid film thickness significantly and the deformations on the gas-liquid interface are small.

4.3. Computation Results

Film and gas Reynolds numbers, heat flux, heater size, channel height, gravity conditions have been varied in the calculations. Liquid film flow take place due to interaction of a number of forces such as gravity force, thermocapillary force that move liquid from the hottest to the coldest regions, shear stress on the gas-liquid interface, because of co-current gas flow, etc. This motion of liquid is characterized by appearance of regions where film becomes thinner or thicker, Fig. 4.1.

Two lateral waves with the length much longer than the heater length are formed near the lateral sides of the heater. Investigations have shown that film deformations and especially film thinning are

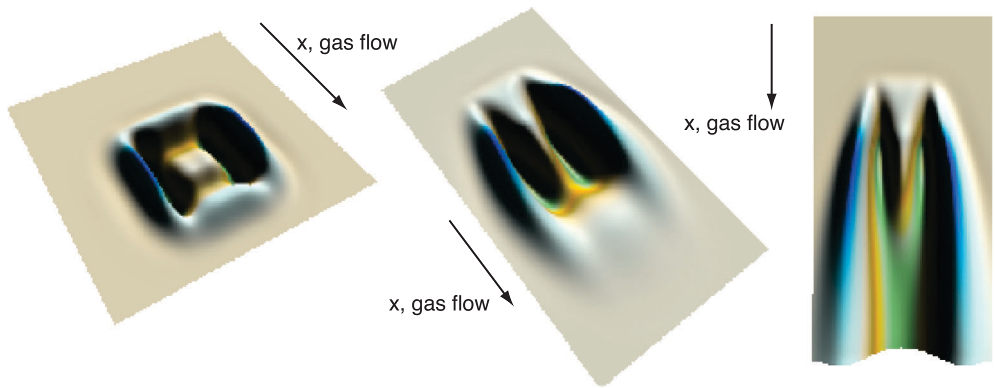

Figure 4.1. Dynamic of gas-liquid interface [94]. Horizontal minichennel, H = 1.4 mm, $Re_l = 5$ (initial film thickness is equal to 103.8 μm), $Re_g = 300$, Bi = 1, $q = 0.25$ W/cm^2. Vector of gravitational acceleration is oriented perpendicular to the flow. Time moments are 0.25 second, 1.25 second and 3.75 s.

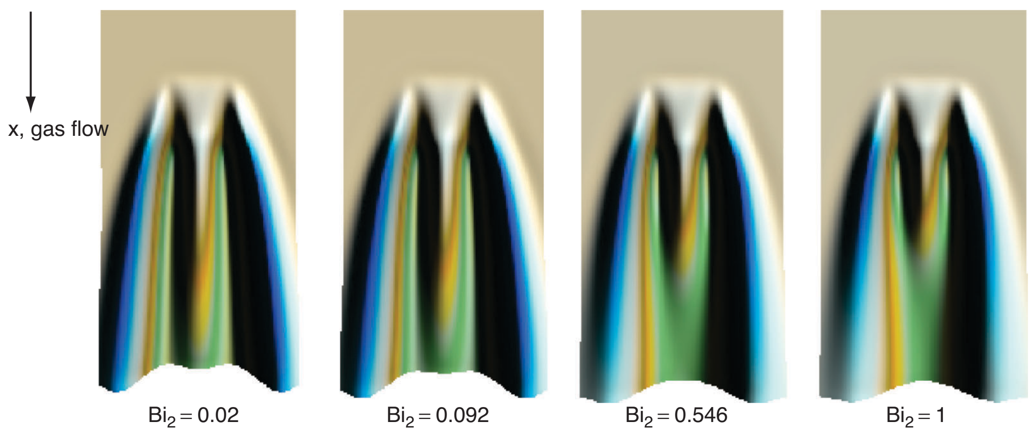

Figure 4.2. Gas-liquid interface position versus Biot numbr. All parameters are the same as in Fig. 4.1, t = 3.75 sec., [94].

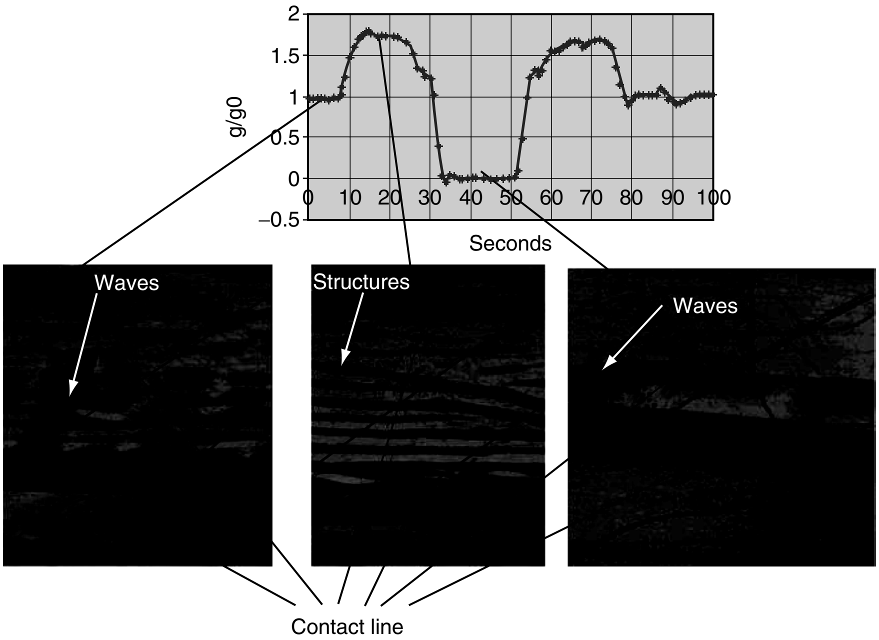

Figure 5.1. Rivulet flow at different levels of gravity, $Q_g = 10$ l/min, $Q_l = 7$ ml/min, T = 20°C, [99].

very sensitive to the liquid, gas and channel parameters and gravity [36, 93]. In some cases film pattern noticeably changes in spanwise direction and a middle stream between two main lateral waves appear. Increasing of heat flux leads to increasing of liquid film deformations. The most dangerous deformations (regions with minimum film thickness and with possible disruption of liquid) take place behind the lower edge of the heater that is well coincides with experimental data (Fig. 4.8a). Liquid bump appears also at the front heater edge. The value of Biot number at the free surface affects the liquid film pattern and location of the region of minimum film thickness, Fig. 4.2.

5. RIVULET FLOWS

Rivulets flowing at mini- and microchannels, as a special case of two-phase flows, can be very promising in earth and space applications [95, 96, 97, 98]. The paper [99] focuses on the recent progress that has been achieved in the understanding of the rivulet flow phenomena through conducting experiments and theory. New experimental results for the shear-driven rivulets of FC-72 were obtained in several parabolic flights campaigns of the European Space Agency as well as in the standard laboratory environments.

It was found theoretically and numerically that the main parameters determining the shape of the rivulet are the contact angle, gravity, the angle of inclination of the substrate to the horizon and the value of the shear stress on the gas-liquid interface. For the gravity-driven rivulet flow regime it was shown that the presence of significant inclination of the surface makes the width of the rivulet less sensitive to the gravity [98].

The experimental results and numerical calculations predict that with the gas flow rate increasing, the width of rivulet decreases. With gas-liquid flow rates ratio increasing the width of rivulet decreases and that for smaller flow rates ratios the rivulet widths is greater. Variations of acceleration during the aircraft manoeuvre and photographs of the rivulet at different levels of gravity are shown in Fig. 5.1. Schlieren visualization for spanwise deformations has been made. The rivulet width increases with the level of gravity. At hyper gravity the width of the rivulet can exceed twice one at microgravity.

It was demonstrated by numerical calculations that with the decreasing of the height of the channel, the influence of the gravity on the rivulet flowing reduces [100]. The main reason for this effect is that the absolute value of the average velocity of the liquid in microchannel increase by a factor 5–10 due to a significant shear stress on the gas-liquid interface increase. Also an uneven distribution of the shear stress on the gas-liquid interface can be important.

6. CONCLUSIONS

The paper provides an overview of the recent progress that has been achieved in the experimental and theoretical investigations of the interfacial thermal fluid phenomena in thin liquid films. It is quite evident that the processes under consideration are controlled by combined effects of evaporation, thermocapillarity, gas dynamics, and gravity as well as by contact –line forces [101, 102, 103] and have not yet been studied systematically. Contrary to gravity-driven liquid films, shear-driven films are less likely to rupture. This provides a way to prevent and control a hot dry patch formation by the shear stress induced by gas flow. A detailed flow sub-regimes map of stratified film flow of FC-72 liquid film and nitrogen gas in 2 mm flat mini-channel and room temperature has been analyzed. It was found that shear-driven and intensively evaporating films are unstable for all liquid/gas flow rates. The flow pattern has quite complicated character and consists of coexisting 2D and 3D waves with different wavelength. For shear-driven liquid films the critical heat flux is up to 10 times higher than that for a falling liquid film, which makes shear driven films (stratified and annular two-phase flow) more suitable for cooling applications than falling liquid films.

ACKNOWLEDGMENT

This work was supported by the Ministry of Education and Science of the Russian Federation in the framework of FTP «Scientific and Scientific-Pedagogical Personnel of the Innovative Russia» in 2009-2013 (state contracts No П1443 and No П362). The author also gratefully acknowledges support of this work by the European Space Agency in the framework of SAFIR PRODEX project (Belgium) and ONR NICOP Grant N00014-08-1-0263.

REFERENCES

[1] Grand-Piteira N., Daerr A., Limat L., Meandering Rivulets on a Plane: A Simple Balance between Inertia and Capillarity, *PRL,* 2006, 96, 254503.

[2] Cazabat A.M., Heslot F., Troian S.M., and Carles P., Fingering instability of thin spreading films driven by temperature gradients, *Nature,* 1990, 346, 824.

[3] Huppert H.E. Flow and instability of a viscous current down a slope, *Nature,* 1982, 300, 427–429.

[4] Joo S.W., Davis S.H., Bankoff S.G., A mechanism for rivulet formation in heated falling films, *J. of Fluid Mechanics*, 1996, 321, 279–298.

[5] Kalliadasis S., Demekhin E.A., Ruyer-Quil C., Velarde M.G., Thermocapillary instability and wave formation on a film falling down a uniformly heated plane, *J. of Fluid Mechanics,* 2003, 492, 303–338.

[6] Miladinova S., Slavtchev S., Lebon G., Legros J.C., Long-wave instabilities of non-uniformly heated falling films, *J. of Fluid Mechanics*, 2002, 453, 153–175.

[7] Oron A., Davis S.H., Bankoff S.G., Long scale evolution of thin liquid films, *Rev of mod physics,* 1997, 69 (3), 931–980.

[8] Alekseenko S.V., Nakoryakov V.E., Pokusaev B.G., Wave flow of liquid films, Begell House Inc., New York, 1994.

[9] Demekhin E.A., Chang H.-C., Complex Wave Dynamics on Thin Films, Elsevier, Amsterdam, 2002.

[10] Kabov O.A., Marchuk I.V., Chupin V.M., Thermal imaging study of the liquid film flowing on vertical surface with local heat source, *Russian Journal of Engineering Thermophysics*, 1996, 6 (2), 104–138.

[11] Kabov O.A., Formation of regular structures in a falling liquid film upon local heating, *Thermophysics and Aeromechanics*, 1998, 5 (1), 547–551.

[12] Kabov O.A., Legros J.C., Marchuk I.V., Scheid B., Deformation of the free surface in a moving locally-heated thin liquid layer, *Fluid Dynamics*, 2001, 36 (3), 521–528.

[13] Kabov O.A., Scheid B., Sharina I.A., Legros J.C., Heat transfer and rivulet structures formation in a falling thin liquid film locally heated, *Int. J. Thermal Sciences*, 2002, 41, 664–672.

[14] Kabov O.A., Scheid B., Kuznetsov V.V., Kabova I.O., Legros J.C., Free surface deformation in a locally heated falling thin liquid film with the temperature dependent viscosity. *Proc. of the 12th Int. Heat Transfer Conference*, Grenoble, 2002, 18–23 August.

[15] Zaitsev D.V., Kabov O.A., Evseev A.R., Measurement of Locally Heated Liquid Film Thickness by a Double-Fiber Optical Probe, *Experiments in Fluids*, 2003, 34, 748–754.

[16] Marchuk I.V., Kabov O.A., Numerical Modeling of Thermocapillary Reverse Flow in Thin Liquid Films under Local Heating, *Russ. J. Eng Thermophysics*, 1998, 8 (1–4), 17–46.

[17] Kuznetsov V.V., Dynamics of locally heated liquid films, *Russ. J. Eng Thermophysics*, 2000, 10 (2), 107–120.

[18] Sharypov O.V., Medvedko K.A., On the stability of a 2D film flow regime with a non-uniform temperature of the free surface, *Russ. J. Eng Thermophysics*, 2000, 10, 315–336.

[19] Scheid B., Oron A., Colinet P., Thiele U., Legros J-C., Nonlinear evolution of nonuniformly heated falling liquid films, *Phys of Fluids*, 2002, 14 (12), 4130–4151.

[20] Skotheim J.M., Thiele U., Scheid B., On the instability of a falling film due to localized heating, *J. Fluid Mech*. 2003, 475, 1–19.

[21] Kalliadasis S., Kiyashko A., Demekhin E.A., Marangoni instability of a thin liquid film heated from below by a local heat source, *J. Fluid Mech*., 2003, 475, 377–408.

[22] Tiwari N., Mester Z., Davis JM., Stability and transient dynamics of thin liquid films flowing over locally heated surfaces, *Physical review E*, 2003, 76 (5), 056306.

[23] A.M. Frank, 3D numerical simulation of regular structure formation in a locally heated falling film, *European Journal of Mechanics B/Fluids*, 2003, 22, 445–471.

[24] Frank M. A. and Kabov O.A., Thermocapillary structure formation in a falling film: Experiment and calculations, *Phys of Fluids*, 2006, 18, 032107.

[25] Kabova Yu.O., Kuznetsov V.V., Kabov O.A., The Effect of Mutual Location of Heaters on the Falling Film Dynamics, *Microgravity sci. technol*., 2007, XIX-3/4, 53–56.

[26] Celata G. P., Colin C., Colinet P., Di Marco P., Gambaryan-Roisman T., Kabov O., Kyriopoulos O., Stephan P., Tadrist L., Tropea C., Bubbles, drops, films: transferring heat in space, *Europhysics News*, 2008, 39 (4), 23–25.

[27] Kabov O.A., Bartashevich M.V., Glushchuk A., Cheverda V. The effect of variable gravity and shear stress on the flattened rivulet dynamics in a minichannel, *1st European Conference on Microfluidics – Microfluidics,* Bologna, December 10–12, 2008, µFLU08-232, 1–11.

[28] Mahajan R., Chiu C., Chrysler G., Cooling a Microprocessor Chip, *Proceedings of the IEEE*, 2006, 94 (8), 1476–1486.

[29] Dae Whan K., Bar-Cohen A., Rahim E., Han B., Thermofluid Characteristics of Two-Phase Flow in Microgap Channels, *Proc. IEEE ITHERM Conference*, Orlando, Florida, May 2008.

[30] Bar-Cohen A., Rahim E., Modeling and Prediction of Two-Phase Microgap Channel Heat Transfer Characteristics, *Heat Transfer Engineering*, 2009, 30 (8), 601.

[31] Bar-Cohen A. and Rahim E., Modeling and prediction of two-phase refrigerant flow regimes and heat transfer characteristics in microap channels, *Proceedings of the 5th International Conference on Nanochannels*, Microchannels and Minichannels, June 18–20, 2007, Puebla, Mexico, 2007.

[32] Bar-Cohen A., Sherwood G., Hodes M., and Solbreken G., Gas-Assisted Evaporative Cooling of High Density Electronic Modules, *IEEE Transactions on Components, Hybrids, and Manufacturing Technology*, 1995, 18 (3), 502–509.

[33] Kabov O.A., Kuznetsov V.V., Legros J-C., Heat transfer and film dynamic in shear-driven liquid film cooling system of microelectronic equipment, *Proc. II Int. Conf. on Microchannels and Minichannels*, Rochester, 2004, 687–694.

[34] Kabov O.A., Lyulin Yu.V., Marchuk I.V. and Zaitsev D.V., Locally heated shear-driven liquid films in microchannels and minichannels, *International Journal of Heat and Fluid Flow*, 2007, 28, 103–112.

[35] Gatapova E.Ya., Kabov O.A., Shear-driven flows of locally heated liquid films, *Int. Journal of Heat and Mass Transfer*, 2008, 51 (19–20), 4797–4810.

[36] Kabova Yu.O., Kuznetsov V.V., Kabov O.A., Gravity effect on the locally heated liquid film driven by gas flow in an inclined minichannel, *Microgravity sci. technol*., 2008, 20, 187–192.

[37] Kabov O.A., Gatapova E.Ya. and Zaitsev D.V., Cooling technique based on evaporation of thin and ultra thin liquid films, *Eleventh Int. Conf. on Thermal and Thermomechanical Phenomena in Electronic Systems, ITherm 2008*, Florida, May 28–31, publication on CD-ROM by IEEE, ISBN:978-1-4244-1701-8, 2008, 520–527.

[38] Kabov O., Cooling of Microelectronics by Thin Liquid Films, Keynote lecture, *Proc. Int. Workshop on "Wave Dynamics and Stability of Thin Film Flow Systems"*, September 1–4, Chennai, India, Narosa Publishing House, 2006, 279–311.

[39] Kabov O.A., Capillary Effects Influence on Vapor Liquid Film Condensation and Heat Transfer in Falling Liquid Film, Doctor of sciences thesis (habilitation), Institute of Thermophysucs, Novosibirsk, June 1999, 283 pages.

[40] Kabov O.A. and Marchuk I.V., Infrared Study of the Liquid Film Flowing on Surface with Nonuniform Heat Flux Distribution, Int. Symposium on The Physics of Heat Transfer in Boiling and Condensation, 21–24 May, Moscow, Russia, 1997, 491–499.

[41] Marchuk I., Infrared study of the liquid film flowing on the substrate with local heat source, Ph.D. thesis, Institute of Thermophysucs, Novosibirsk, 2000.

[42] Scheid B., Kabov O.A., Minetti C., Colinet P. and Legros J.C., Measurement of free surface deformation by reflectance-schlieren technique, Proc. 3-rd European Thermal Sciences Conference, 10–13 September 2000, Heidelberg, 2000, 1, 651–657.

[43] Nusselt W. Die Oberflachen-Kondensation des Wasserdampfes, Zeitschrift der VDI., 1916., 27., 541–546, 1916, 28, 569–575.

[44] Kabov O.A. and Chinnov E.A., Heat Transfer From a Local Heat Source to a Subcooled Falling Liquid Film Evaporating in a Vapor-Gas Medium, *Russian Journal of Engineering Thermophysics*, 1997, 7 (1–2), 1–34.

[45] Kabov O.A., Legros J.C., Muzykantov A.V., Tereshenko A.G., Zaitsev D.V., The Influence of surface inclination angle and Reynolds number on the wavelength of the regular structures formed by local heating of gravitationally falling liquid film, Proc. Joint Meeting 4th Workshop on Transport Phenomena in Two-Phase Flow, 11–16 Sept. 1999, Sozopol, Bulgaria, 1999, 243–250.

[46] Taylor G., The instability of liquid surfaces when accelerated in a direction perpendicular to their planes, *Proc. Roy. Soc. Ser. A*, 1950, 201 (1065), 192–196.

[47] Bellman R. and Pennington R.H., Effects of Surface Tension and Viscosity on Taylor Instability, *Quarterly of Applied Mathematics*, 1954, 12, 151–162.

[48] Scriven L.E. and Sterling C.V., On Cellular Convection Driven by Surface Tencion Gradients: Effect of Mean Surface Tension and Surface Viscosity, *J. Fluid Mech.*, 1964, 19, 321–340.

[49] Chinnov E.A., Kabov O.A., Jet formation in gravitational flow of a heated wavy liquid film, *Journal of Applied Mechanics and Technical Physics*, 2003, 44 (5), 708–715.

[50] Chinnov E.A., Kabov O.A., Marchuk I.V., and Zaitsev D.V., Heat transfer and breakdown of subcooled falling liquid film on a vertical middle size heater, *Intern. Journal Heat and Technology*, 2002, 20 (1), 69–78.

[51] Chinnov E.A. and Kabov O.A. The Effect of three-dimensional deformations on local heat transfer to a nonuniformly heated falling film of liquid, *High Temperature*, 2004, 42 (2), 267–277.

[52] Marchuk I.V. and Kabov O.A., Measurements of liquid film surface temperature under thermocapillary structured flows, Book of Abstracts of Int. Marangoni Association Congress, Brussels, July 14–17, 2004, 66–67.

[53] Zaitsev D.V. and Kabov O.A. Study of the thermocapillary effect on a wavy falling film using a fiber optical thickness probe, *Experiments in Fluids*, 2005, 39 (4), 712–721.

[54] Chinnov E.A. and Kabov O.A., Marangoni Effect on Wave Structure in Liquid Films, *Microgravity sci. technol.*, 2007, XIX-3/4, 18–22.

[55] Chinnov E.A., Nazarov A.D., Kabov O.A., Serov A.F., Measurement of the wave characteristic of a non-isothermal liquid film by the capacitance probe, *Thermophysics and Aeromechanics*, 2004, 11 (3), 441–447.

[56] Chinnov E.A., Nazarov A.D., Saprykina.A.V., Serov A.F., Influence of thermocapillary effects on wave characteristics of the heated liquid film, *Thermophysics and Aeromechanics*, 2007, 14 (1), 67–74.

[57] Kabov O.A., Marchuk I.V., Saprikina A.V. and Chinnov E.A., Temperature pulsations and thermocapillary effects in the wavy heated liquid film, *Fluid dynamics,* 2008, 4, 108–117.

[58] Kabov O.A., Breakdown of a liquid film flowing over the surface with a local heat source, *Thermophysics and Aeromechanics*, 2000, 7 (4), 513–520.

[59] Zaitsev D.V., Kabov O.A., Cheverda V.V., and Bufetov N.S, The Effect of Wave Formation and Wetting Angle on the Thermocapillary Breakdown of a Falling Liquid Film, *High Temperature*, 2004, 42 (3), 450–456.

[60] Zaitsev D., Thermocapillary Rupture of Falling Liquid Films, Ph.D. thesis, Institute of Thermophysics SB RAS, Novosibirsk, Russia, 2003.

[61] Gimbutis I., Heat Transfer to a Falling Fluid Film, Mokslas, Vilnius, 1988.

[62] Chinnov E.A., Kabov O.A., Muzykantov A.V., Zaitsev D.V., Influence of plate inclination on heat transfer and breakdown of locally heated flowing liquid film, *Intern. Journal of Heat and Technology*, 2001, 19 (1), 31–44.

[63] Zaitsev D.V. and Kabov O.A., Falling Liquid Film Breakdown on Heated Substrate, XXVII Siberian Seminar on Thermalphysics, 1–5 October, Novosibirsk, 2004, publication on CD-ROM, paper 055, 1–19 (in Russian).

[64] Zaitsev D.V., Semenov A. and Kabov O.A., Viscosity Effect on Thermocapillary Rupture of Falling Liquid Films, Proceedings of Int. Heat Transfer Conference, IHTC14, August 8–13,Washington, DC, 2010, paper: IHTC14-23222.

[65] Hartley D.E., Murgatroyd W., Criteria for the Break-Up of Thin Liquid Layers Flowing Isothermally Over Solid Surfaces, *Int. J. Heat Mass Transfer*, V. 7. P. 10031964.

[66] Zuber N., Staub F.W**,** Stability of Dry Patches Forming in Liquid Films Flowing Over Heated Surface, *Int. J. Heat Mass Transfer*, V. 9. P. 897, 1966.

[67] Ruckenstein E**.,** On the Break-Up of Thin Liquid Layers Flowing Along a Surface, *Int. J. Heat Mass Transfer*, V. 14. P. 165, 1971.

[68] El-Genk M.S., Saber H.H., Minimum thickness of a flowing down liquid film on a vertical surface, *Int. J. Heat Mass Transfer*, V. 44. P. 2809, 2001.

[69] El-Genk M.S., Saber H.H., An investigation of the breakup of an evaporating liquid film, falling down a vertical, uniformly heated wall, *J. of Heat Transfer*, 2002, 124, 39.

[70] Zaitsev D.V., Rodionov D.A., Kabov O.A., Study of thermocapillary film rupture using a fiber optical thickness probe, *Microgravity sci. technol.*, 2007, XIX-3/4, 100–103.

[71] Zaitsev D.V. and Kabov O.A., An experimental modeling of gravity effect on rupture of a locally heated liquid film, *Microgravity sci. technol.*, 2007, XIX-3/4, 174–177.

[72] Gatapova E.Ya., Zaitsev D.V. and Kabov O.A., Role of Thermocapillary Convection in Rupture of a Falling Liquid Film Heated from Below, Proceedings of ASME 2010 3rd Joint US-European Fluids Engineering Summer Meeting and 8th Int. Conference on Nanochannels, Microchannels, and Minichannels, FEDSM2010-ICNMM2010, August 1–5, Montreal, 2010, paper FEDSM-ICNMM2010-31264.

[73] Taitel Y., Duckler A.E., A model for predicting flow regime transitions in horizontal and near horizontal gas-liquid flow, *AICHE Journal*, 1976, 22 (1), 47.

[74] Chinnov E.A. and Kabov O.A., Two phase flow in pipes and capillary channels. Review, *High temperatures*, 2006, 44(5), 777–795.

[75] Kabov O.A. and Bar-Cohen A., Cooling technique based on evaporation of thin liquid films in microgap channels, *ECI Int. Conf. on Boiling Heat Transfer*, Florianópolis-SC-Brazil, 3–7 May, Keynote lecture KN13, publication on CD-ROM, 2009, 1–6.

[76] Yang, Y., Fujita, Y., Flow boiling heat transfer and flow pattern in rectangular channel of mini-gap, *Second International Conference on Microchannels and Minichannels,* New York, USA, 2004. ICMM2004-2383.

[77] Cortina-Diaz M., and Schmidt J., Flow Boiling Heat Transfer of n-Hexane and n-Octane in a Minichannel, *Proc. the 13th International Heat Transfer Conference, Sydney, Australia*, 2006.

[78] Kabov O.A., Zaitsev D.V., Effect of shear stress and gravity on rupture of a locally heated liquid film, *Multiphase Science and Technology*, 2009, 21 (3), 249–266.

[79] Zaitsev D.V. and Kabov O.A., Microgap cooling technique based on evaporation of thin liquid films, *Proc. of IPACK2009*, July 19–23, 2009, San Francisco, publication on CD-ROM, 2009, paper IPACK2009-89318, 1–7.

[80] Kabov O.A., Chinnov E.A. and V. Cheverda, Two-phase flow in short rectangular mini-channel, *Microgravity sci. technol.*, 2007, XIX-3/4, 44–47.

[81] Chinnov E.A. and Kabov O.A., Two-phase flow in a short mini-channel, *Technical Physics Letters,* 2008, 34 (16), 41–47.

[82] Chinnov E.A., Guzanov V.V., Cheverda V., Markovich D.M and Kabov O.A., Regimes of Two-Phase Flow in Short Rectangular Channel, *Microgravity sci. technol.*, 2009, 21 (1), S199-S205.

[83] Chinnov E.A. and Kabov O.A., Features of two-phase flow in a rectangular microchannel, *Technical Physics Letters,* 2010, 36 (5), 468–470.

[84] Coleman J.W and Garimella S., Characterization of two-phase flow patterns in small diameter and rectangular tubes, *Int. J. Heat and Mass Transfer*, 1999, 42, 2869–2881.

[85] Kabov O.A., Bartashevich M.V., Glushchuk A., Cheverda V. The effect of variable gravity and shear stress on the flattened rivulet dynamics in a minichannel, *1st European Conference on Microfluidics - Microfluidics 2008* - Bologna, 2008, December 10–12, paper μFLU08-232.

[86] Cheverda V. and Kabov O.A., Flow regimes map for FC-72 liquid film in the rectangular mini channel, *Third Int. Topical Team Workshop on Two-Phase Systems for Ground and Space Applications, Brussels, Sept. 10–12, Book of Abstracts*, 2008, 97.

[87] Gatapova, E. Ya., Kabov, O.A., Kuznetsov, V.V., Legros, J.-C., Evaporating shear-driven liquid film flow in minichannel with local heat source, *J. Eng. Thermophys.*, 2005, 13 (2), 179–197.

[88] Gatapova E.Ya., Kabov O.A., Marchuk I.V., Thermocapillary Deformation of a Locally Heated Liquid Film Moving under the Action of a Gas Flow, *Technical Phys. Let.*, 2004, 30 (5), 418–421.

[89] Gatapova E.Ya., Thermocapillary Convection in Locally Heated Liquid Film Moving under the Action of Gas Flow, Ph.D. thesis, Institute of Thermophysics SB RAS, Novosibirsk, Russia, 2005.

[90] Kabova, I.O. and Kuznetsov, V.V., Downward flow of a nonisothermal thin liquid film with variable viscosity (in Russian); English transl. in *Journal of Applied Mechanics and Technical Physics*, 2002, 43 (6), 895–901.

[91] Kabova, I.O., Thermocapillary deformation of a nonisothermal flowing liquid film, *Technical Physics Letters*, 2004, 30 (5), 432–434.

[92] Kabova Yu.O., Flow of nonisothermal liquid films on smooth and microstructured substrates, Ph.D. thesis, Lavrentyev Institute of Hydrodynamics SB RAS, Novosibirsk, Russia, 2006.

[93] Kabova Yu.O., Kuznetsov V.V., Kabov O.A., The Effect of Mutual Location of Heaters on the Falling Film Dynamics, *Microgravity sci. technol.* 2007, XIX-3/4, 53–56.

[94] Kabova Yu.O., Kuznetsov V.V. and Kabov O.A., The effect of gravity and shear stress on a liquid film driven in a horizontal minichannel at local heating, *Microgravity sci. technol.*, 2009, 21 (1), S145-S152.

[95] Alekseenko S.V., Antipin V.A., Bobylev A.V., Markovich D.M., Application of PIV to velocity measurements in a liquid film flowing down an inclined cylinder, *Exp.Fluids*, 2007, 43, 197–207.

[96] Gambaryan-Roisman T., Stephan P., Flow and Stability of rivulets on heated surfaces with topography, *Journal of Heat Transfer*, 2009, 131, 033101-1-033101-6.

[97] Bartashevich M.V., Kuznetsov V.V. and Kabov O.A., Mathematical modeling of rivulet flow driven by variable gravity and gas flow in a minichannel, *Proceedings of the 6th Int. Conf. on Nanochannels, Microchannels and Minichannels, ICNMM2008*, Darmstadt, 2008, June 23–25, Germany.

[98] Bartashevich M.V., Kuznetsov V.V., Kabov O.A., The rivulet flowing in inclined minichannel with co-current gas flow in conditions of variable gravity, *Sib. Zh. Ind. Mat.,* 2009, 12 (2(38)), 3–16. (In Russian).

[99] Kabov O.A., Bartashevich M.V. and Cheverda V., Rivulet flows in microchannels and minichannels, *Proc. of 7th Int. Conf. on Heat Transfer, Fluid Mechanics and Thermodynamics*, Keynote lecture, 19–21 July 2010, Antalya, 2010.

[100] Bartashevich M.V., Kuznetsov V.V., Kabov O.A., Dynamics of the restricted liquid film in co-current gas flow in microchannel, *Fluid Dynamics*, 2010.

[101] Potash M. and Wayner P.C., Evaporation from a two-dimensional extended meniscus, *Int. J. Heat Mass Transfer*, 1972, 15, 1851–1863.

[102] Stephan P. and Brandt C., Advanced capillary structures for high performance heat pipes, *Proc. I Int. Conf. on Microchannels and Minichannels*, Rochester, NY, 2003, April 24–25, 69–75.

[103] Ajaev V.S., Spreading of thin volatile liquid droplets on uniformly heated surfaces, *J. Fluid Mech.*, 2005, 528, 279–296.